THE ASTROPHYSICAL JOURNAL, 376:380–403, 1991 August 1
© 1991. The American Astronomical Society. All rights reserved. Printed in U.S.A.

WINDS, OUTFLOWS, AND INFLOWS IN X-RAY ELLIPTICAL GALAXIES. I.

LUCA CIOTTI
Dipartimento di Astronomia, Università di Bologna, CP 596, I-40100, Bologna, Italy
ANNIBALE D'ERCOLE
Osservatorio Astronomico di Bologna, CP 596, I-40100, Bologna, Italy
AND
SILVIA PELLEGRINI AND ALVIO RENZINI[1]
Dipartimento di Astronomia, Università di Bologna, CP 596, I-40100, Bologna, Italy
Received 1990 July 6; accepted 1991 January 24

ABSTRACT

A new class of one-dimensional hydrodynamical evolutionary sequences for the gas flows in elliptical galaxies is presented. The model galaxies are described by either King's or de Vaucouleurs's virialized density distributions, constrained to lie on the *fundamental plane* of elliptical galaxies, and are surrounded by variable amounts of dark matter. Two source terms operate: mass loss from evolving stars, and a secularly declining heating by Type I supernovae. The resulting models evolve through up to three consecutive evolutionary stages: the wind, outflow, and inflow phases. Agreement with the observed trends of the X-ray luminosity L_X, with the optical characteristics of the galaxies, is achieved for dark-to-visible mass ratios of ~ 10, when the standard SN I rate is assumed. Also the large dispersion of L_X for given optical luminosity is easily accounted for. These sequences indicate that the X-ray faint galaxies are still in their wind phase, while the bulk of ellipticals are in the outflow phase, and a few of the brightest galaxies may have already experienced their transition to the inflow regime. In models with a de Vaucouleurs distribution small *mini-inflows* can be present in the central regions long before the global transition to the main inflow regime. The effects of interactions with the intracluster medium, ram pressure, encounters, and merging events are qualitatively discussed. We argue that the iron abundance in the flows can constrain the SN I heating rate in the galaxies, while the total mass of iron in the intracluster medium provides a constraint on the total number of Type I SNs so far exploded in cluster galaxies. Our adopted SN I rate implies a total iron mass in excellent agreement with current estimates for nearby clusters. Finally, the $L_X - L_B$ correlation is seen as an ongoing manifestation of the fact that brighter galaxies are characterized by a larger binding energy per unit mass, i.e., as an implication of the Faber-Jackson $L_B - \sigma_*$ relation, not unlike the L_B-metallicity correlation established at the formation epoch of elliptical galaxies.

Subject headings: dark matter — galaxies: evolution — galaxies: structure — galaxies: X-rays — stars: supernovae

1. INTRODUCTION

As first revealed by *Einstein* observations, normal (non-cD) elliptical galaxies, both isolated or belonging to groups and clusters, can be powerful X-ray sources (Forman et al. 1979), with 0.5–4.5 KeV luminosities L_X ranging from $\sim 10^{39}$ to $\sim 10^{42}$ ergs s^{-1} (Forman, Jones, & Tucker 1985; Canizares, Fabbiano, & Trinchieri 1987, hereafter CFT; see also Fabbiano 1989 for an extended review).

The X-ray emission is found to correlate strongly with the optical luminosity of the observed galaxies (e.g., CFT find $L_X \propto L_B^{1.7\pm 0.3}$), but there is substantial scatter at any luminosity, as shown in Figure 1. The scatter is about a factor of 50 for $L_B \simeq 5 \times 10^{10}\ L_\odot$, and to account for the dispersion of the X-ray properties at any optical luminosity is at least as important as to explain the average correlation. Moreover, for $L_B \lesssim 3 \times 10^{10}\ L_\odot$ the observed L_X is consistent with an emission due entirely to discrete sources (see also CFT), while only for larger luminosities is there compelling evidence for an additional contribution from a hot interstellar medium (ISM).[2]

Again, reducing the empirical evidence to just the average correlation may misleadingly suggest that the gas flows in ellipticals are qualitatively all the same, with just quantitative differences between one galaxy and another. Detailed information on the X-ray surface brightness distribution exists for only a handful of elliptical galaxies, which in these cases turns out to be close to the optical distribution (Trinchieri, Fabbiano, & Canizares 1986, hereafter TFC). Assuming the gas density profile of these three objects to be typical for all early-type galaxies, from the observed L_X values the total mass of the emitting gas can then be derived. Typical values are thus found in the range $M_{\rm gas} = 10^8$–$10^{11}\ M_\odot$ (Fabbiano 1989).

New optical data for large and homogeneous samples of elliptical galaxies have recently become available, thus allowing a more elaborated approach than formerly possible, when only the correlation of the total luminosity (e.g., L_B) with the central velocity dispersion σ_* was considered (Faber & Jackson 1976). Thus, elliptical galaxies appear to lie close to a fundamental plane (FP) in the space of the basic observables: total luminosity (e.g., L_r or L_B), central velocity dispersion (σ_*) and average (effective) surface brightness—either $\langle \mu_r \rangle_e$ or $\langle \mu_B \rangle_e$—(Lauer 1985; Dressler et al. 1987, hereafter 7SI; Djorgovski & Davis 1987, hereafter DD). In this frame, using the 7SI diameter-velocity dispersion relation as a distance indica-

[1] Also European Southern Observatory.

[2] The actual contribution of the discrete sources is still matter of debate. We have adopted $L_{\rm discr} = 1.5 \times 10^{40}\ L_B/10^{11}\ L_\odot$ ergs s^{-1}, i.e., the lower envelope of the data points in Fig. 1. This is about one-half of the value adopted by CFT and ~ 4 times larger than postulated by Forman et al. (1985).

© American Astronomical Society • Provided by the NASA Astrophysics Data System

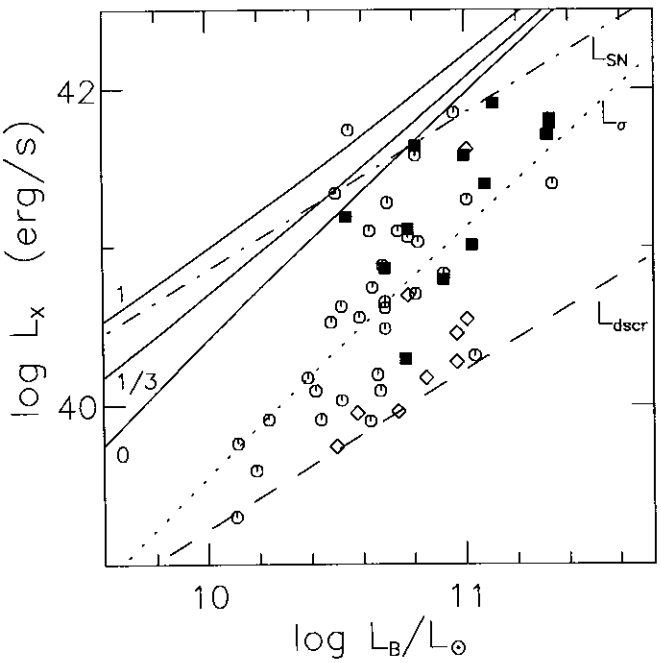

FIG. 1.—The X-ray vs. blue luminosity for early-type galaxies from Canizares, Fabbiano, & Trinchieri (1987). Filled squares and open diamonds refer to galaxies with boxy and disklike isophotal shapes, respectively. Open circles represent galaxies for which this morphological detail is unknown. The dot-dashed line shows the power L_{SN} generated by the SN I heating at the standard rate ($\vartheta_{SN} = 1$). The heating due to stellar motions L_σ is shown by the dotted line, while L_{dscr} represents the expected contribution from discrete stellar X-ray sources (*dashed line*). Finally, the solid lines represent the expected X-ray luminosity of steady state cooling flow models ($L_{inflow} = L_{SN} + L_\sigma + L^+_{grav}$), for the indicated values of the SN parameter ϑ_{SN}.

tor, Donnelly, Faber, & O'Connell (1990) re-examine the correlation of X-ray and optical luminosities. With the new distances the slope of L_X vs. L_B is slightly increased ($L_X \propto L_B^{2.18}$), and the scatter is significantly reduced (by $\sim 20\%$), partly thanks to improved photometry from Faber et al. (1989). However, whether the new distances are more accurate than those adopted by CFT remains a matter of debate, with implications far beyond the problem of the X-ray luminosity of elliptical galaxies (see Silk 1989; Djorgovski, de Carvalho, & Han 1989). Whatever the true scale is, a large scatter of L_X for each L_B remains also in the Donnelly et al. study, and remains one of the main observational facts to be explained.

The X-ray luminosity of ellipticals as seen in the framework of the FP is further explored by Djorgovski & de Carvalho (1989), who conclude that the X-ray ellipticals do not occupy or avoid any special region of the FP, and there is a marginal reduction in scatter when correlating L_X with a linear combination of σ_* and $\langle\mu\rangle_e$, instead with L_B. Correlations with apparently minor morphological details have also been investigated: Bender et al. (1989) find a correlation between the X-ray luminosity and the *boxiness* parameter a_4/a. Galaxies with $a_4/a < 0$ have boxy isophotes, while those with $a_4/a > 0$ have a pointed, disklike shape. The claimed correlation is in the sense of boxy galaxies being stronger X-ray emitters than disklike galaxies, which is interpreted in favor of a connection between the properties of gas flows and merging phenomena. This possibility is also advocated by Djorgovski & de Carvalho (1990), while Donnelly, Faber, & O'Connell (1990) find no statistically significant correlation. In Figure 1 boxy and disklike galaxies are shown with different symbols. Boxiness tends to be confined to optically bright galaxies, which in turn are also brighter in X-rays, while a correlation between L_X/L_B and boxiness appears to be marginal, certainly affected by small number statistics. So, the question remains whether boxiness is primarily related to the optical or to the X-ray luminosity.

The most direct evidence for the presence of a massive ISM in ellipticals comes from X-ray observations, but optical and infrared data can give valuable information on gas phases other than the $\sim 10^7$ K phase. *IRAS* observations give direct information on the dust content of these galaxies and therefore provide indirect evidence for a cold (~ 100 K) atomic and molecular phase, whose total amount remains affected by substantial uncertainties. Typical values range between 10^7 and $10^8\ M_\odot$ (Jura 1990). Neutral hydrogen 21 cm observations of ellipticals have generally given rather low upper limits, but recently Bregman, Roberts, & Giovanelli (1988) have reported the detection of $\sim 10^8\ M_\odot$ in the nearby galaxy NGC 4406. Besides cold red giant winds (which are certainly present), in a few galaxies the cold phase may in addition represent material which has cooled from the hot phase. In some cases there also appears to be nonindigenous cold gas recently captured from a gas-rich dwarf galaxy (e.g., Bertola, Galletta, & Zeilinger 1985). The presence of a warm phase ($\sim 10^4$ K) is revealed by Hα and other emission line observations (e.g., Sadler 1988; di Serego Alighieri, Trinchieri, & Brocato 1990). The latter authors find a typical mass of only a few $10^5\ M_\odot$, distributed in little droplets with small filling factor but large covering factor, all characteristics which naturally apply to the red giant wind material in transit toward the hot phase. In conclusion, the hot phase appears to dominate the ISM of elliptical galaxies by a large margin, while the warm and cold phases may represent material currently in the transition toward the hot phase. Since we are primarily concerned with the dynamics of the hot X-ray emitting gas we shall give less attention to the cooler phases, which, however, represent an important component in the gas metabolism of elliptical galaxies.

Evolving stars shed large amounts of mass, thus rising the important question of how and where elliptical galaxies manage to dispose this gas. At an early stage, models of supernova-driven galactic winds were developed in order to explain the apparent lack of gas inferred from radio and optical observations (Mathews & Baker 1971; MacDonald & Bailey 1981; White & Chevalier 1983). However, supernova-driven galactic wind models fall short by up to four orders of magnitude in L_X and were later abandoned. To prevent the development of galactic winds one can either deepen the gravitational potential well of these galaxies (e.g., by assuming the presence of massive dark halos), or reduce the supernova heating (Nulsen, Stewart, & Fabian 1984). Ever since, the high X-ray luminosity of several elliptical galaxies has indeed been taken as the best evidence for the presence of dark matter in these galaxies (e.g., Sarazin 1987). A wider class of steady state flow models was then explored. This class did not include subsonic outflows, because such flows are unstable and tend to turn into either supersonic winds or inflows, depending on whether heating dominates over cooling, or vice versa, i.e., steady models can describe only gas inflows or supersonic winds. Having excluded winds for the reasons above, inflows remained the only option left, and "cooling flow" models have been extensively investigated (e.g., Nulsen, Stewart, & Fabian 1984; Fabian, Nulsen, & Canizares 1984; Sarazin & White

© American Astronomical Society • Provided by the NASA Astrophysics Data System

1987, 1988; Vedder, Trester, & Canizares 1988). Since these models are nearly hydrostatic over most of the galaxies, large amounts of hot gas can be accommodated in them, and they are therefore very bright in X-rays.

Cooling flow models, however, are far from giving a satisfactory account of the X-ray properties of all elliptical galaxies, as most of them are much fainter than the models would predict (see Fig. 1). This is specially true for homogeneous inflow models (see, e.g., Sarazin & White 1988), but serious problems are also encountered by inhomogeneous models. We postpone an extensive discussion of this aspect to § 2.5, and here we emphasize just the need to explore a wider class of solutions than either steady state winds or cooling flows. This requires us to relax the steady state approximation, therefore adopting a fully evolutionary approach. Evolutionary, hydrodynamical calculations, including the time dependence of the source terms, were first constructed by Mathews & Loewenstein (1986, hereafter ML) and Loewenstein & Mathews (1987a, b [hereafter LM]). LM allowed for the time evolution of the stellar mass-loss rate but assumed a nearly constant rate of Type I SNs (the only type yet observed to occur in ellipticals). LM models develop an inflow from the very beginning, but their ultimate fate is to revert such inflows into outflows (which would soon develop into a supersonic wind), as the stellar mass loss rate secularly declines while the SN heating remains nearly constant. These models are less affected by the X-ray overluminosity syndrome plaguing steady state cooling flow solutions, although at least in part this comes from LM having assumed a stellar mass-loss rate and a SN I rate which are both nearly a factor of ~ 4 lower than standard values. Hattori, Habe, & Ikeuchi (1987) postulate a strictly constant SN I rate, and also their models start with inflows which tend to evolve into partial outflows, outflows, and eventually winds.

As pointed out by LM and Mathews (1988a), in all these models over a Hubble time an amount of material comparable to the mass of stars in the galactic core flows into the nucleus, while the resulting distortions of the central optical surface brightness and velocity dispersion are not observed. Moreover, inflow models exhibit very high central X-ray surface brightness, with the X-ray profile being much more centrally concentrated than the optical profile, at variance with the observed distributions of the three well-resolved galaxies (TFC; Sarazin & White 1988).

A way out from all the above difficulties may come from relaxing the conservative assumption of a virtually constant SN rate over the whole history of the galaxies, and instead allowing for a sizable secular decline (Renzini 1989). Evolutionary sequences of hydrodynamical models which incorporate a secularly declining SN I rate have been constructed by D'Ercole et al. (1989, hereafter Paper I) and reveal that under this assumption elliptical galaxies can experience up to three subsequent evolutionary phases, in which an initial supersonic wind is followed by a subsonic outflow until a central cooling catastrophe leads eventually to the onset of an inflow. This new class of evolutionary solutions exhibits the opposite behavior compared to that explored by either LM or Hattori et al. and presents several advantages over such models. In particular, the duration of the transient outflow phase turns out to be extremely sensitive to virtually every model structural parameter, thus offering a natural explanation for the large scatter in X-ray luminosities.

In this paper we present an extensive selection of evolutionary sequences belonging to this class. In § 2 we describe the main physical ingredients of our models, which include the adopted spatial distributions of both the visible and the dark matter, and the source terms, i.e., the stellar mass loss and the supernova heating. We also discuss the resulting evolution of the energy budget and the origin of some of the difficulties encountered by cooling flow models. Then the basic flow equations and an outline of the numerical methods adopted to integrate them are given in § 3. In § 4 we present the evolutionary sequences relative to model galaxies characterized by a King-law density profile for the visible matter, while § 5 refers to model galaxies following the de Vaucouleurs $r^{1/4}$-law surface brightness distribution. In § 6 we discuss the effects of an intracluster medium on the gas flows in individual galaxies, addressing also the question of the effects of interactions with other galaxies. In § 7 we discuss the major properties of our evolutionary sequences in the light of the available X-ray data and speculate about the fate of infalling matter in those models which present a central inflow. Our conclusions are summarized in § 8.

2. MODEL GALAXIES AND SOURCE TERMS

In this section we describe the procedures adopted for the construction of the bright and dark matter distributions within our model galaxies, and how the model parameters are constrained to produce structures resembling real galaxies. The bright and dark mass distributions being assumed to be time independent, the only secularly evolving ingredients are the source terms: stellar mass loss and supernova heating. We ignore possible heating by energetic particles which may be injected by nuclear activity (e.g., Rephaeli 1987).

2.1. *King and de Vaucouleurs Model Galaxies*

As in previous evolutionary- or stationary-flow studies we neglect the effects of stellar mass loss and gas flows on the gravitational potential well. Also neglected are interactions with surrounding galaxies which might affect the distribution of matter. For the first group of models, which we call King Galaxies (KGs), we assume the stellar distribution to be described by the same density profile used by LM and Sarazin & White (1987). Following the same notations, we call r_{c*}, $r_t = \delta r_{c*}$, and ρ_{*0}, respectively, the core radius, the tidal radius, and the central stellar density. The quantities ρ_{*0} and r_{c*} are further related to the central velocity dispersion σ_* by the virial condition $\rho_{*0} r_{c*}^2 = 9\sigma_*^2/4\pi G$ (e.g., Binney & Tremaine 1987). The stellar velocity dispersion profile $\sigma_*(r)$ is the same as in equation (23) of Sarazin & White (1987), which is valid for an isotropic velocity dispersion.

The second set of galaxy models (dVGs) is described by the de Vaucouleurs $r^{1/4}$-law stellar profiles (as approximated by Mellier & Mathez 1987) truncated at $r_t = \delta r_e$, where r_e is the effective (half-light) radius of the galaxy. We also adopt a *nuclear radius* r_n inside which $\rho_*(r) = \rho_*(r_n)$ is assumed to be constant, so as to avoid the central divergence. For KG models and also for dVG models we use the virial theorem to relate the total stellar mass to the central velocity dispersion; following DD, we adopt from Poveda (1958) $M_* \simeq 7.2 \times 10^2 r_e \sigma_*^2$, where r_e is in parsecs, M_* is the total stellar mass in solar units and σ_* is in km s^{-1}; we also adopt $\sigma_*(r) = \text{const}$.

In both KG and dVG models the density distribution of the dark matter halo is assumed to follow a quasi-isothermal law. As in LM and Sarazin & White (1987), r_{ch} and ρ_{h0} are the core radius and the central halo density, and the tidal radius is assumed to be the same as for the stellar distribution. So, two

© American Astronomical Society • Provided by the NASA Astrophysics Data System

parameters are required to describe the dark matter distribution: $R = M_h/M_*$, which is the ratio of the dark halo mass to the total stellar mass, and for the second parameter either $\gamma = \rho_{h0}/\rho_{*0}$ (the ratio of central dark-matter to stellar-matter density) for the KGs, or $\beta = r_{ch}/r_e$ for the dVGs.

With these assumptions each model is identified by six independent parameters, i.e., (L_B, σ_*, r_{c*}, δ, R, γ) and (L_B, σ_*, r_e, δ, R, β), respectively, for KG and dVG models. Furthermore, one of these parameters can be eliminated by imposing a condition that the model galaxies lie on the fundamental plane, for which we adopt the equation:

$$L_B = 3.6 \times 10^3 r_e \sigma_*^{1.3}/h \quad L_\odot , \tag{1}$$

where r_e is in parsecs, σ_* is in km s^{-1}, and $h = H_0/100$ (Djorgovski & de Carvalho 1989). For all the KG models we have assumed $r_e = 12 r_{c*}$. In conclusion, we identify each KG model by the independent parameters (L_B, σ_*, δ, R, γ), and each dVG model by (L_B, σ_*, δ, R, β). The parameter $\beta = r_{ch}/r_{c*}$ can be introduced for the KG models too, being univocally determined by R, γ, and δ. Perfect symmetry between the two sets of parameters can thus be recovered. Other properties of the galaxy models used in this paper are fully described elsewhere (Ciotti & Pellegrini 1991).

2.2. *Stellar Mass Loss*

In a stellar population stars restitute mass to the ISM at a rate which is given by the product of the stellar death rate $b(t)$ times the average amount of mass which is lost by each dying star. In a single-age stellar population this is given by

$$\dot{M}_*(t) = b(t)\Delta M = \psi(M_{TO})\,|\dot{M}_{TO}|\,\Delta M \quad M_\odot \text{ yr}^{-1} , \tag{2}$$

where ψ is the initial mass function (IMF), $M_{TO}(t)$ is the turnoff mass of the population, and $\Delta M = M_{TO} - M_f(M_{TO})$, with M_f being the final mass, or mass of the remnant left by stars of initial mass M_{TO}. For $M_{TO}(t)$ we use the approximation given by Renzini & Buzzoni (1986). For the initial mass-final mass relation $M_f(M_{TO})$ we adopt the relation given in Table 1, for which a concise justification is appropriate. The final mass is derived from the brightest asymptotic giant branch (AGB) stars in a population of known age (and then known M_{TO}), via the core-mass luminosity relation for thermally pulsing AGB stars (Paczyński 1970; Iben & Renzini 1983). Therefore, in order of increasing initial mass, the final mass is derived from the observed luminosity of brightest AGB stars in galactic globular clusters (Renzini & Fusi Pecci 1988), in billion years old clusters in the Magellanic Clouds (Mould & Aaronson 1985), and in the Magellanic Cloud fields (Mould & Reid 1987). For further justifications of these choices see Wood & Faulkner (1987), and Renzini (1988). For $M > 9\,M_\odot$ we finally assume that stars leave 1.4 $M_\odot$ neutron star remnants. This initial mass–final mass relation is somewhat different from that given by Iben & Renzini (1983) and incorporates some of the modifications advocated by Weidemann (1984). We estimate these values of M_f to be accurate to within a few $10^{-2}\,M_\odot$ (in particular for low values of M_i), and therefore ΔM remains determined with a better than 10% accuracy.

It may be important to realize how narrow is the mass range relevant to most of the cosmological evolution of a passively evolving population, past the first few 10^8 yr (see Table 2). Therefore, past the first $\sim 10^9$ yr what matters is the behavior of the IMF within the fairly restricted mass range ~ 0.85–$1.75 M_\odot$. We adopt $\psi(M) = AM^{-(1+x)}$, and to connect

TABLE 1

$M_{TO} - M_f$ RELATION

M_{TO}	M_f	ΔM
0.85	0.55	0.30
2.0	0.60	1.40
3.0	0.80	2.20
5.0	0.85	4.15
9.0	1.06	7.94

the scale factor A (giving the size of the stellar population) to the present galaxy luminosity L_B we make use of our knowledge of the specific evolutionary flux of the stellar population, i.e., $B(t) = b(t)/L_T$ (L_T is its total bolometric luminosity), and therefore $b(t) = AM_{TO}^{-(1+x)}\,|\dot{M}_{TO}| = B(t)L_T$. For the present age of the model galaxies we assume $t = 15$ Gyr, and correspondingly $B \simeq 2 \times 10^{-11}\ L_\odot^{-1}\ \text{yr}^{-1}$, fairly independent of either the IMF slope or composition (Renzini & Buzzoni 1986). Next one needs a relation between L_T and L_B, and following Greggio & Renzini (1990) we adopt $L_T \simeq 2.4 L_B$ as typical for an average elliptical galaxy. We caution, however, that this coefficient is sensitive to both the age and, especially, the metallicity distribution of the stellar population (see Buzzoni 1989) and is likely to represent the main uncertainty in the derived rate of mass return. Using these values in the expression above for $b(t)$, and evaluating for $t = 15$ Gyr and $x = 1.35$ the terms containing M_{TO}, one finally obtains $A = 2.9 L_B$. We stress that throughout the whole paper by L_B we mean the blue luminosity at $t = 15$ Gyr, i.e., by definition the *present* luminosity. In this way we finally obtain:

$$\dot{M}_*(t) = -2.9 L_B M_{TO}^{-2.35}\,|\dot{M}_{TO}|\,\Delta M \quad M_\odot \text{ yr}^{-1} . \tag{3}$$

For quick calculations one can use the approximation $\dot{M}_*(t) \simeq -1.5 \times 10^{-11} L_B t_{15}^{-1.3}$ (where t_{15} is the age in units of 15 Gyr), valid in the range from ~ 0.5 to over 15 Gyr. Note that in this range the time exponent is fairly insensitive to variations of the IMF slope (Mathews 1989), a result of the narrow range in M_{TO} spanned by the corresponding populations (see Table 2). The quantity actually entering into the hydrodynamical calculations is the specific rate of mass return $\alpha_* = \dot{M}_*/M_*$ (see § 3.1). As noted in Paper I, there is a significant discrepancy between the present estimate and that adopted by others (e.g., LM's α_* is a factor ~ 3.5 smaller). We consider our estimate to be very robust at, say, the 15% level, even including the uncertainty in the blue to bolometric conversion for elliptical galaxies. For $t = 15$ Gyr the present estimate is in excellent agreement with that of Faber & Gallagher (1976).

TABLE 2

RATES OF STAR DEATHS, MASS RETURN, AND SUPERNOVAE[a]

Time (Gyr)	M_{TO} ($M_\odot$)	ΔM ($M_\odot$)	$b(t)$ (yr^{-1})	$R_{SN}(t)$ (yr^{-1})	b/R_{SN}	$\dot{M}_*$ ($M_\odot$ yr^{-1})	Fe/Fe$_\odot$
0.2	3.18	2.5	124	9.3	13.3	310	7.5
0.5	2.22	1.6	72	2.6	27.8	115	5.6
1.0	1.75	1.15	45	1.0	46.1	52	4.7
2.0	1.40	0.82	27	0.37	73.1	22	4.1
5.0	1.09	0.53	13	0.10	127	6.9	3.7
10.0	0.92	0.37	7	0.04	184	2.6	3.7
15.0	0.85	0.30	5	0.02	219	1.5	3.7

[a] For a galaxy with $L_B = 10^{11}\,L_\odot$, IMF slope $1 + x = 2.35$, and supernova rate parameters $\vartheta_{SN} = 1$ and $s = 1.4$.

© American Astronomical Society • Provided by the NASA Astrophysics Data System

2.3. *Supernova Heating*

The second evolving ingredient in our model galaxies is the supernova heating. It is well known that only Type I SNs (actually Type Ia) have so far been observed in elliptical and S0 galaxies (e.g., Tammann 1982). In the passive aging of a coeval stellar population Type II SN events are confined to the first ~ 20 million yr. Later, only Type I SNs remain to provide energy input into the ISM, and therefore the secular evolution of their rate takes control over such input. Note that our sequences of evolutionary hydrodynamical models actually start at $t = 10^8$ yr, well after the last Type II SN has exploded in the model population.

The rate of Type Ia SNs past an initial burst of star formation depends on the nature of the precursors. Two competing scenarios are currently being investigated, and both involve carbon deflagration in a white dwarf that exceeds the Chandrasekhar limit as a result of mass accretion from a binary companion. In the *single degenerate* (SD) model (Whelan & Iben 1973) the companion is a living, evolved star which fills its Roche lobe and pours matter onto the WD. Thus the explosion time delay is set by how long it takes to the companion to evolve and fill its Roche-lobe, which in practice is very close to its evolutionary lifetime $t(M_2)$. The corresponding SN rate is

$$R_{\rm SD} = \psi_s[M_2(t)]\,|\,\dot{M}_2\,|\,, \tag{4}$$

where ψ_s is the mass function of the secondary components of those binary systems which produce a SN Type Ia. As for the flux $b(t)$, the rate is given by the product of a distribution function, ψ_s, times a clock rate. The clock is indeed the same as in equation (2): it is the thermonuclear clock controlling stellar lifetimes, i.e., $M_2(t) = M_{\rm TO}(t)$, as the initial mass of components filling their Roche lobe at time t is virtually the same as the turnoff mass of the coexisting population of single stars.

In the double degenerate (DD) model (e.g., Iben & Tutukov 1984) also the companion is a WD, and the explosion occurs when the two WDs merge as a result of angular momentum losses via gravitational wave radiation (GWR). The explosion time is now set by $t(M_2)$ plus the GWR delay $t_{\rm GWR}(a_0)$ taken by the two WDs to spiral in until merging. From Landau & Lifshitz (1951):

$$t_{\rm GWR}(a_0) = \frac{1.5 \times 10^8 a_0^4}{M_1 M_2 (M_1 + M_2)}\ {\rm yr}\,, \tag{5}$$

where a_0 is the semimajor axis of the system at the formation of the second WD (in $R_\odot$ units). If $t_{\rm GWR} \ll t(M_2)$, then GWR is so fast that it does not introduce any further appreciable delay before explosion, and $R_{\rm DD} \simeq R_{\rm SD}$ as given by equation (4). In the opposite limit, $t_{\rm GWR} \gg t_2(M_2)$, the SN I rate is given by

$$R_{\rm DD} = \psi_a[a_0^m(t)] \times \dot{a}_0^m\,, \tag{6}$$

where ψ_a is the distribution function of the initial separation of the DD systems and $a_0^m(t)$ the initial separation of those DDs that merge at time t, i.e., the inverse function of $t_{\rm GWR}(a_0)$. Note the close formal similarity between the expressions for $R_{\rm DD}$ and $R_{\rm SD}$, with the distribution ψ_a taking the place of the initial mass function ψ_s and the GWR clock $\dot{a}_0^m$ replacing the thermonuclear clock $|\,\dot{M}_{\rm TO}\,|$. Note that in both cases the run of the clock is very well known, while all the complicacies of the binary statistics and evolution make the modulators ψ_s and ψ_a virtually unknown. For example, only direct observations of close WD + WD pairs can give useful indications about the ψ_a factor (see Bragaglia et al. 1990).

It is worth emphasizing that for much of the evolution of our model galaxies, e.g., from $t = 1$ to 15 Gyr, what matters is the behavior of ψ_s between $\sim 1\ M_\odot$ and $\sim 2\ M_\odot$ for the SD model, and of ψ_a between $\sim 1.7\ R_\odot$ and $\sim 3\ R_\odot$ for the DD model. It would be surprising if either ψ_s or ψ_a were to change by very large factors within such narrow ranges. This argument suggests the clock rate (either $\dot{M}_{\rm TO}$ or $\dot{a}_0$) as the main factor controlling the time evolution of the SN I rate. Indeed, the two clocks slow down considerably between 1 and 15 Gyr, the stellar clock by a factor ~ 50 and the GWR clock by a factor ~ 8. For either model we then expect a sizable reduction of the SN I rate with cosmological time, unless the modulating factors closely balance the drop of the clock rate. For example, in the SD model of Greggio & Renzini (1983) ψ_s favors more massive secondaries, and $R_{\rm SD}$ drops by a factor ~ 100 between 1 and 15 Gyr (Renzini 1989). We conclude that a secularly declining SN I rate follows quite plausibly from current theoretical views, and we correspondingly assume:

$$R_{\rm SN}(t) = 2.2 \times 10^{-13} \vartheta_{\rm SN} L_B t_{15}^{-s}\ \ {\rm yr}^{-1}\,, \tag{7}$$

where $\vartheta_{\rm SN}$ is a parameter. For $\vartheta_{\rm SN} = 1$ and $t_{15} = 1$ the standard SN I rate in ellipticals is recovered, i.e., 0.22 SNU (1 SNU = 1 SN per century per $10^{10}\ L_\odot$; Tammann 1982). For reasons that will become clear in the next subsection, we assume s values such that $R_{\rm SN}$ decreases slightly faster than α_*. In practice, this implies $s \gtrsim 1.3$, for the adopted IMF slope $1 + x = 2.35$. We further assume that each SN injects into the ISM a total kinetic energy $E_k = 10^{51}$ ergs. Therefore, the global SN heating (hereafter SN luminosity) is given by

$$L_{\rm SN}(t) = E_k R_{\rm SN}(t) \simeq 7.1 \times 10^{30} \vartheta_{\rm SN} L_B t_{15}^{-s}\ \ {\rm ergs\ s^{-1}}\,. \tag{8}$$

Besides energy, SN I's provide also mass and heavy elements. We assume that each SN I ejects $1.4\ M_\odot$, while the total mass-specific rate of mass return becomes $\alpha = \alpha_* + \alpha_{\rm SN}$, with $\alpha_{\rm SN}(t) = 1.4\ R_{\rm SN}(t)/M_*$, (e.g., LM; ML; Paper I). Of each SN ejecta, a mass $M_{\rm Ni} \simeq 0.5\ M_\odot$ is in the form of radioactive ^{56}Ni, which ultimately decays into iron (see Woosley & Weaver 1986). Notice that there is a direct link between the amount of Ni ejected, the total thermonuclear energy released, and the part of it which goes into kinetic energy of the ejecta (the total energy released minus the binding energy of the WD). Following Arnett, Branch, & Wheeler (1985) $E_k \simeq 10^{51}$ $(3.1\ M_{\rm Ni} - 0.5)$ ergs, and for $M_{\rm Ni} \simeq 0.5\ M_\odot$ we can adopt $E_k \simeq 2 \times 10^{51}\ M_{\rm Ni}$ ergs. As ^{56}Ni decays to iron, the bulk of the fresh iron produced by each SN I event is $M_{\rm Fe} \simeq M_{\rm Ni}$, or perhaps $\sim 20\%$ larger (see Woosley & Weaver 1986), and the iron abundance in the hot galactic flows becomes

$$Z_{\rm flow}^{\rm Fe} = \langle Z_*^{\rm Fe} \rangle + \frac{M_{\rm Fe} R_{\rm SN}}{\dot{M}_*}\,, \tag{9}$$

where $\langle Z_*^{\rm Fe} \rangle$ is the mass-loss–averaged iron abundance of the stars of the galaxy. This latter quantity can in principle be obtained via population synthesis techniques, while the iron abundance in the flows can be obtained from the X-ray iron lines. So, in principle one can gather fairly direct information on the SN heating by comparing the iron abundance in the flows to that of the stars, i.e., independently of estimates of the SN rate. To further illustrate the case, we introduce the quantity:

$${\rm Fe}^{\rm ex} = \frac{M_{\rm Fe} R_{\rm SN}(t)}{\dot{M}_* Z_\odot^{\rm Fe}} \simeq 1.5 \times 10^{-2} \vartheta_{\rm SN} M_{\rm Fe} t_{15}^{1.3-s} / Z_\odot^{\rm Fe}\,, \tag{10}$$

© American Astronomical Society • Provided by the NASA Astrophysics Data System

which is the excess iron abundance in the flow due to SN I contamination.

In Table 2 we report the time dependence of several quantities so far introduced in this section, for a representative galaxy with $L_B = 10^{11}\ L_\odot$, $\vartheta_{SN} = 1$ and $s = 1.4$. As a function of time in column (1), columns (2) and (3) give the turnoff mass M_{TO} and the corresponding mass loss ΔM. Columns (4) and (5) give the single star death rate $b(t)$ and the SN rate, respectively. The ratio $b(t)/R_{SN}(t)$ (i.e., the number of dying single star per SN event) is next given in column (6). Finally, columns (7) and (8) give the rate of mass return and the excess iron abundance in the ISM, from equation (10) with $M_{Fe} = 0.5\ M_\odot$ and $Z_\odot^{Fe} = 0.002$ (for this latter value, see Anders & Grevesse 1989). Clearly the iron content in our model flows can be up to several times solar. We shall return to this question in § 7.

On the observational side, the determination of the SN rate in ellipticals remains a difficult undertaking. The *canonical* rate of 0.88 h^2 SNU has been sometimes regarded as extremely uncertain, yet it is worth emphasizing that the other existing estimates agree surprisingly well after all. Cappellaro & Turatto (1988) give, in fact, 0.69 h^2 SNU; Evans, van den Bergh, & McClure (1989) give 0.32 h^2 SNU; and van den Bergh & Tammann (1991) adopt an even larger value, 0.98 h^2, or $\vartheta_{SN} = 1.1$. All in all, it seems to us worth concluding that the rate may be uncertain by a factor of 2, perhaps 3; while the order of magnitude uncertainty occasionally advocated has at the moment no empirical basis. Concerning the uncertainty induced by a possible systematic distance error, we notice that the estimated kinetic energy release by one SN event scales approximately as h^{-2} (Arnett et al. 1985), and therefore the SN luminosity, as given by equation (8), is virtually unaffected by a systematic error in the distance scale. Finally, concerning the time evolution of the SN rate (as described by the parameter s), valuable support to the notion of a strong evolution (i.e., large value of s) is provided by the pronounced correlation with the galactic star formation rate, as the rate of Type Ia SNs per unit near IR luminosity appears to increase by an order of magnitude along the Hubble sequence, i.e., from ellipticals to late spirals (van den Bergh 1991).

2.4. *Evolution of the Energy Budget*

Having described the structure of the model galaxies and the source terms which operate in them, we have all we need for a close examination of the global energy balance of the resulting galactic flows. Collisions between stellar winds, and/or between winds and ambient gas are supposed to thermalize the kinetic energy carried by the winds. The global power provided to the ISM by this *kinetic heating* is

$$L_\sigma = \tfrac{3}{2}\alpha(t)\int_0^{r_t} 4\pi r^2 \rho_*(r)\sigma_*^2(r)dr\ , \qquad (11)$$

where $\sigma_*(r)$ is the local, one-dimensional velocity dispersion. We define L_{grav}^- as the power required to steadily extract from the galaxy the gas shed by stars, and L_{grav}^+ as the power generated by the steady inflow of this gas through the galactic potential well, down to the center of the galaxy. Thus we have

$$L_{grav}^- = -\alpha(t)\int_0^{r_t} 4\pi r^2 \rho_*(r)\phi(r)dr\ , \qquad (12)$$

$$L_{grav}^+ = \alpha(t)\int_0^{r_t} 4\pi r^2 \rho_*(r)[\phi(r) - \phi(0)]dr\ . \qquad (13)$$

The integrals appearing in these definitions can be expressed as a product of two terms: a dimensional factor, and a dimensionless function of R, β, and δ:

$$L_{grav}^\pm = \alpha(t)M_*\sigma_*^2 F^\pm(R,\beta,\delta) \simeq \dot{M}_*(t)\sigma_*^2 F^\pm(R,\beta,\delta)\ . \qquad (14)$$

The dimensionless form factors $F^\pm$ are different functions of (R, β, δ), respectively, for the KG models (with $\beta = r_{ch}/r_{c*}$ and $\delta = r_t/r_{c*}$), and for the dVG models (with $\beta = r_{ch}/r_e$ and $\delta = r_t/r_e$). The time dependence of $L_{grav}^\pm$ is totally controlled by $\alpha(t)$, while the other terms describe the properties of the potential well. The exact form of the $F^\pm$ functions is given in Ciotti & Pellegrini (1991), but for quick estimates we give here some useful approximations. For both KG and dVG models F^- is well described by a relation of the type $F^- = A(\delta) + B(\beta,\delta) \times R = 8.26\tilde{F}^-(R,\beta,\delta)$. When expressing σ_* in units of 300 km s^{-1}, and including into F^- all other numerical coefficient, for the KG models we have

$$\tilde{F}_K^-(R,\beta,\delta) \simeq 0.336(\delta/140)^{-0.16} + 0.089(\beta/10)^{-0.14}(\delta/140)^{-0.6}R\ . \qquad (15)$$

Seemingly, for the dVG models (with $\beta = \frac{3}{8}$ and $\delta = 15$) one can use $\tilde{F}_{dV}^-(R) = 0.24 + 0.069R$.

We now introduce the function $\chi(t)$, as the ratio of the power required to steadily extract the gas from the galaxy, to the power actually made available by kinetic and supernova heating; so for both KG and dVG models we have

$$\chi(t) = \frac{L_{grav}^-(t)}{L_\sigma(t) + L_{SN}(t)} \simeq \frac{t_{15}^{s-1.3}}{\vartheta_{SN}} \times \left(\frac{\sigma_*}{300}\right)^2 \times \tilde{F}^-(R,\beta,\delta)\ , \qquad (16)$$

where we have used equation (8), and neglected α_{SN} in front of α_*, and L_σ in front of L_{SN} (this latter assumption leads to a $\sim$10% overestimate of χ). Equation (16) separates the stellar evolution terms from the galactic structure terms and helps distinguishing the relative role of the various parameters. So, the first term contains the SN-related parameters ϑ_{SN} and s the second term (σ_*^2) gives a first hint to the depth of the potential well, which is then fully determined after multiplication with the third term, which contains the dark matter–related parameters R and β. Using the function $\chi(t)$ one can now distinguish four main possible evolutionary behaviors of the gas flows. To case 1 belong model galaxies in which at any time $\chi(t) < 1$. The opposite situation we call case 2, with $\chi(t) > 1$ at any time. Case 3 galaxies are defined as those in which initially $\chi(t) > 1$, but χ secularly *decreases* until at some time $\chi(t) < 1$. Finally, case 4 is the opposite of case 3, with χ *increasing* with time, from initial values below unity, to a final value above unity. The actual evolutionary behavior of type 1 galaxies can be somewhat affected by the choice of initial conditions, but they are energetically able to sustain a supersonic wind from the beginning all the way to the present. On the contrary, in type 2 model galaxies a wind is energetically impossible, and an inflow is established over the whole time interval. Type 3 galaxies will initially host an inflow, but as χ decreases below unity the tendency will be to turn the inflow into an outflow, and eventually into a supersonic wind. Finally, the opposite tendency will be exhibited by type 4 galaxies, with initial winds turning later into inflows, after χ has increased above unity. So, apart from environmental effects, $\chi > 1$ is a *sufficient* condition for galaxies to host an inflow, while $\chi < 1$ is a *necessary* condition for them to maintain a wind.

Type 1 galaxies contain little gas at any time, and so they cannot account for the X-ray properties of many present day

© American Astronomical Society • Provided by the NASA Astrophysics Data System

TABLE 3

VALUES OF $\chi\vartheta_{SN}$ AT $t = 15$ GIGAYEARS

	KG MODELS			dVG MODELS		
R	$\sigma_* = 200$	$\sigma_* = 300$	$\sigma_* = 400$	$\sigma_* = 200$	$\sigma_* = 300$	$\sigma_* = 400$
0....	0.16	0.37	0.66	0.13	0.29	0.52
3....	0.30	0.67	1.19	0.24	0.55	0.97
6....	0.43	0.97	1.72	0.35	0.80	1.42
9....	0.56	1.26	2.25	0.47	1.05	1.88
12....	0.69	1.56	2.77	0.58	1.31	2.33

ellipticals. Type 2 galaxies correspond to inflow models, and it is also well known that such models tend to predict too large X-ray luminosities (see § 3.5). Type 3 galaxies have been already investigated for the case of a practically constant SN rate (LM). In the present investigation we are concerned with type 4 model galaxies, basically the only one which has not been previously investigated.

Present values of $\chi(t_{15} = 1)$ are given in Table 3 for various choices of the galactic parameters. We note that for $\vartheta_{SN} = 1$ and low values of R one has $\chi \ll 1$ for every reasonable combination of the parameters, i.e., with the standard SN rate and without dark matter all galaxies would sustain a supersonic wind, and the classical Mathews & Baker (1971) result is recovered. We also note that for low σ_* (low L_B) the present χ is less than unity with the standard SN rate, i.e., there is ample energy input to sustain a supersonic wind even with ~ 10 times more dark than visible matter, and low X-ray luminosities are predicted. On the contrary, at the opposite extreme ($\sigma_* \gtrsim 300$ km s^{-1}), one has $\chi \gtrsim 1$ even for modest amounts of dark matter, SN heating may be insufficient to prevent inflows, and large X-ray luminosities are then expected. For intermediate luminosities, a transition between the two regimes has necessarily to take place, and a large sensitivity of L_X to the galactic model parameters is therefore anticipated.

2.5. *Energetic Embarrassments of Cooling Flow Models*

When the gas lost by stars is allowed to flow freely down to the center of the galaxy (such as in homogeneous cooling flow models) the global rate at which energy has to be radiated away is given by

$$L_{\rm inflow} \simeq L_\sigma + L^+_{\rm grav} + L_{\rm SN} \,. \tag{17}$$

This assumes that the whole potential energy of the gas is radiated during inflow, while insofar as the flow is nearly hydrostatic, the virial theorem requires that only half of this energy is radiated. However, toward the center a cooling flow departs dramatically from hydrostaticity (it actually becomes supersonic!) and cools to very low temperatures thus radiating all its internal energy. Which additional fraction of $L^+_{\rm grav}$ is further radiated, and which fraction survives as kinetic energy of the condensed residue of the flow, depend on the unknown details of the condensation process (e.g., star formation). It is fair to state that more (and possibly much more) than 50% of $L^+_{\rm grav}$ is indeed radiated. Given the high temperature in the flow, most of the emission is in the X-ray band, and an X-ray luminosity $L_X \simeq L_{\rm inflow} + L_{\rm dscr}$ is expected (e.g., CFT). In Figure 1 $L_{\rm inflow}$ is displayed for three values of ϑ_{SN}, having connected σ_* to L_B via the Faber-Jackson relation. One can see that complete inflow models are far too bright in X-rays than indicated by the observations, a well-known embarrassment (see for example Fig. 1 in Sarazin & White 1988). These latter authors also note that in lower luminosity galaxies the gas temperature is lower, and a significant fraction of the emitted radiation is softer than X-rays. From their Figure 1 we estimate that for $L_B = 10^{10}\, L_\odot$ the reduction of L_X over $L_{\rm inflow}$ is negligible for the case $\vartheta_{SN} = 1$ and may be as large as a factor ~ 2.5 for the case $\vartheta_{SN} = 0$.

In an attempt to reduce the X-ray output of homogeneous cooling flow models, a major reduction of the SN rate has been first advocated. For example, Thomas (1986) adopts a rate 20 times lower than the standard rate, and yet one does not achieve the desired reduction. Indeed, Figure 1 shows that even with no supernovae at all ($\vartheta_{SN} = 0$) $L_{\rm inflow}$ is still too large: when all the gas falls in then too much gravitational energy is liberated, and too much X-ray luminosity is produced. This proves that in most galaxies the bulk of the gas does not flow from the production site, all the way to the center. In order to preserve the cooling flow scenario thermal instabilities have been supposed to induce local condensations, with the bulk of the gas dropping out of the flow at large radii (e.g., Thomas 1986; Sarazin & Ashe 1989). From Figure 1 we notice that the required reduction in L_X is on average much larger in optically faint galaxies than in bright galaxies, and the efficiency of thermal instabilities should correspondingly be much larger in faint galaxies with a low-density ISM, compared to bright galaxies with a massive ISM. Moreover, such an efficiency should exhibit macroscopic galaxy to galaxy variations, so as to account for the large dispersion in L_X/L_B ratios. Neither of these two requirements has yet received a physical justification. Moreover, Sarazin & Ashe (1989) estimate that thermal instabilities can reduce L_X by at most a factor less than 3 and conclude that variations in their efficiency cannot be responsible for the full range in the observed X-ray luminosities. Therefore, even inhomogeneous cooling flow models do not provide a satisfactory account for the observed X-ray properties.

Apart from these astrophysical difficulties, the ability of thermal instabilities to drop matter out of the flow in normal ellipticals remains physically conjectural. Loewenstein (1989) finds that overdensities by a factor of 10 or more would be required for cooling out to occur, given the stabilizing effect of buoyancy. This effect could be suppressed by magnetic fields causing the local perturbations to comove with the flow, but Loewenstein (1990) finds that the conditions favorable to the growth of thermal instabilities are fairly restrictive in the case of cluster cooling flows, while the case of flows in individual ellipticals remains to be investigated. That thermal instabilities cannot solve the problem of the excess X-ray luminosity is further illustrated by the fact that even postulating a drastic reduction in both $L_{\rm SN}$ and $L^+_{\rm grav}$, still one would have $L_X \simeq L_\sigma + L_{\rm dscr}$, which remains considerably in excess of the observed L_X of many galaxies (see Fig. 1). For such galaxies the only way of saving the cooling flow scenario is to postulate a major reduction of the *effective* rate of mass return from evolving stars, which in principle could be achieved either by reducing $\dot{M}_*$ below the values given by equation (3), or by assuming that the bulk of the gas lost by stars never joins the hot ISM, but rather cools off *in situ* disappearing into unobservable condensations. For the reasons given in § 2.2 one can definitely rule out the former option. Concerning the second option, Thomas (1986) suggests that stellar mass loss may consist of localized $\sim 1\, M_\odot$ blobs expanding from the central star, which immediately recondense locally without ever being heated to X-ray

© American Astronomical Society • Provided by the NASA Astrophysics Data System

temperatures. This is a rather unrealistic description of stellar mass loss and its interaction with the hot X-ray gas. Evolving stars in a 15 Gyr old population have an initial mass of ~ 0.85 $M_\odot$, and each star loses in total ~ 0.30 $M_\odot$ via low-velocity winds during the RGB and the AGB phases of evolution. Typical mass-loss rates are a few 10^{-8} $M_\odot$ yr^{-1} for such stars, and the mass-loss process correspondingly lasts for some 10^7 yr. During this time the mass losing star is orbiting at a few hundred kilometers per second w.r.t. the hot phase, thus covering distances of several kiloparsecs. It is hard to figure out how ~ 1 $M_\odot$ blobs could be formed under such conditions, and Mathews (1990) and Renzini (1990) conclude that stellar ejecta unavoidably join the hot phase. Given the failure of both homogeneous and inhomogeneous cooling flow models, we have therefore started exploring a wider class of solutions, in which the a priori assumption of a pure inflow is relaxed, also winds and outflows are allowed, and a fully evolutionary approach is adopted.

3. THE HYDRODYNAMICAL MODELS

3.1. *Hydrodynamical Equations and Their Integration*

To describe the evolution of the hot gas we solve the time-dependent, Eulerian equations of gasdynamics with source terms, that we write in the form:

$$\frac{\partial \rho}{\partial t} + \nabla \cdot (\rho v) = \alpha \rho_* , \tag{18}$$

$$\frac{\partial m}{\partial t} + \nabla \cdot (mv) = -(\gamma - 1)\nabla E - g\rho , \tag{19}$$

$$\frac{\partial E}{\partial t} + \nabla \cdot (Ev) = -(\gamma - 1)E\nabla \cdot v - L + \alpha \rho_* \left(\epsilon_0 + \frac{1}{2} v^2 \right), \tag{20}$$

where ρ, m, and E are, respectively, the density of mass, momentum, and internal energy of the gas, and v is the fluid velocity, $\gamma = 5/3$ is the ratio of the specific heats, and g is the gravitational acceleration due to the total mass distribution (stars and dark halo). Finally, $\epsilon_0 = 3kT_0/2\mu m_p$ is the injection energy per unit mass, T_0 is the injection temperature (see, e.g., LM for more details), and $L = n_e n_p \Lambda(T)$ is the cooling rate per unit volume. For the cooling law $\Lambda(T)$ we follow the prescriptions of Mathews & Bregman (1978). The positive source term on the right-hand side of the energy equation describes the heating of the gas by supernova blast waves and by the relative motion of the mass-losing stars and the ISM (kinetic heating).

To integrate this set of equations we have used an improved version of the code described by Bedogni & D'Ercole (1986). It is an Eulerian, first-order, upwind scheme on which several gestures toward second-order accuracy are implemented. The control-volume formulation is used, and in addition to slab averages, independent slab-average gradient values represent the distribution of convected quantities (van Leer 1977). The grid has typically 100 zones and extends up to 500 kpc. In order to get a reasonable spatial resolution in the inner region of the model galaxies we adopted a geometrical progression for the mesh size, the first mesh being 100 pc wide. The whole evolution is usually covered in $\sim 10^5$ times steps for the KG models, while dVG sequences may require up to 10 times more time steps in order to satisfy the Courant condition and other stability constraints near the center. At the outer boundary usual outflow conditions are assumed, while reflecting boundary conditions are adopted at the center. Mainly for computational reasons, the gas temperature is not allowed to drop below 10^4 K, so as to avoid an excessive reduction on the time steps when rapid cooling is present near the center. Such an assumption does not affect our conclusions, but—as in the case of previous similar calculations—it prevents us from following the detailed behavior of the cooling gas at low temperatures.

3.2. *Initial Conditions*

We assume the model galaxies to be initially devoid of gas, i.e., $\rho(r) = 0$ for $t = 0$. This is certainly a simplification of the real physical situation in the early evolutionary stages of elliptical galaxies, when intense star formation has necessarily to take place. In this way only the gas originated by stellar mass loss is actually considered, while any residual primordial gas could greatly enhance the radiation losses and affect the behavior of the gas flow which is being established. There are, however, reasonable astrophysical justifications for this assumption. The intense star formation activity during the early evolution of elliptical galaxies was certainly accompanied by a high rate of SN explosions, primarily Type II SNs produced by massive stars. According to the classical models of Larson (1974), during this early stage the energy injection into the ISM provided by Type II supernovae becomes sufficient to unbound the residual gas, and a galactic wind is established. This scenario has several attractive characteristics, e.g., (1) it is able to account for the luminosity-metallicity correlation among elliptical galaxies (Larson 1974; Tinsley 1980; Arimoto & Yoshii 1987; Matteucci & Vettolani 1988) and (2) it agrees with the clear evidence that at some stage galaxies are able to eject large amounts of nuclearly processed materials, as demanded by the observed high metallicity of the intracluster medium (e.g., Rothenflug & Arnaud 1985, and references therein).

Our initial condition $\rho(r) = 0$ is therefore equivalent to assume that galactic winds are established by SN activity (mainly Type II), early in the evolution of elliptical galaxies. The same assumption is made in other evolutionary hydrodynamical models (e.g., LM), and also in our sequences the early phase preceding the establishment of the galactic wind is not followed at all, primarily because one is concerned with the hot gas phase, and no allowance is made for cool (molecular) gas and ongoing star formation. The early evolutionary stages of our models ($t \lesssim$ few 10^8 yr) will then bear little resemblance to real primordial galaxies but should give a more realistic representation of the subsequent evolution, once a wind is established and the gas flows *lose memory* of the specific events responsible for the establishment of such winds. In practice we started the calculations at $t = 10^8$ yr, also to avoid the unphysical divergences in equations (7) and (8).

As emphasized earlier in this paper, one distinct aspect of our approach is the attention payed to supernovae of Type I. When only Type II SNs are considered, the SN heating practically ceases when the star formation rate drops to zero. This results from the short lifetime of SN II precursors ($\sim 10^7$ yr). As a consequence, galactic models which include only Type II SNs will tend to exhibit strong intermittencies in the star formation rate, because Type II SNs trigger a wind thus inhibiting further star formation, the SN rate drops, the wind stalls, a new burst of star formation becomes possible, and a new cycle begins (e.g., Arimoto 1989; Hensler & Burkert 1990). Such intermittencies can be avoided when Type I SNs are included in the model, as they ensure the continuation of the SN heating even long after any star formation has ceased.

© American Astronomical Society • Provided by the NASA Astrophysics Data System

TABLE 4

KG MODELS: INPUT PARAMETERS

Model	L_B ($10^{11}\,L_\odot$)	σ_* (km s^{-1})	δ	R	$10^2\gamma$
K1	0.5	280	180	9	1.25
KRM	0.5	270	180	9	1.25
KRMa	0.5	270	180	5.8	0.81
KRMb	0.5	270	180	15	2.2
K2a	0.5	265	150	9	1.25
K2b	0.5	265	180	9	1.25
K2c	0.5	265	180	9	0.125
K2d	0.5	265	180	9	0.5
K3	0.5	260	180	9	1.25
K4	0.5	220	180	9	1.25
K5	1	280	180	9	1.25
K6a	1	260	150	9	1.25
K6b	1	260	180	9	1.25
K7	1	250	180	9	1.25

NOTE.—For all models $\vartheta_{SN} = \frac{2}{3}$, except for KRMa and KRMb, for which $\vartheta_{SN} = \frac{1}{2}$ and $\vartheta_{SN} = 1$, respectively.

4. THE KG EVOLUTIONARY SEQUENCES

In this section we present the results of the hydrodynamical calculation of gas flows in the KG models. We first illustrate in some detail the main characteristics of the evolving flow in one specific case, that we call the *reference model* (hereafter KRM). We then explore the KG parameter space, commenting on the effects of changing each parameter with respect to the KRM.

4.1. *Evolution of the Gas Flow in the Reference Model*

The KRM is determined by the set of parameters given in Table 4. From the FP (with $h = \frac{1}{2}$) and virial equations several other characteristics of the KRM remain determined, e.g., the total stellar mass, the central stellar density ρ_{*0}, the (stellar) core radius r_{c*}, and the tidal radius r_t which are all given in Table 5. For the SN parameters we adopt $(\vartheta_{SN}, s) = (\frac{2}{3}, 1.5)$, a choice for which initially $\chi \ll 1$ (i.e., $L_{SN} \gg L_{grav}$), and there is ample SN heating to sustain a supersonic wind. Then χ increases above unity at $t \simeq 2.5$ Gry, and keeps monotonically increasing till the present, when $\chi(15) = 1.14$.

Figure 2 displays the radial behavior of the gas velocity, temperature, and density at different epochs in the course of the evolution of the flow. The flow is initially highly supersonic, with the sonic point located at $r \simeq 1$ kpc, but rapidly moving outward as the whole flow decelerates as a result of the decreasing injection temperature (decreasing supernova heating). In this way, by $t = 1.5$ Gyr the sonic point has already reached the edge of the galaxy at $r = r_t = 66.3$ kpc, where it stays for a while, i.e., the flow becomes subsonic inside the galaxy ($r < r_t$), while it remains supersonic outside it ($r > r_t$; see Fig. 3). Then the flow further decelerates with time, becoming more and more subsonic, and the gas configuration inside the galaxy approaches an almost hydrostatic structure: the hot gas is slowly inflated by the supernova heating. During the first ~ 5 Gyr the gas density continuously drops inside the galaxy, as a result of the decreasing rate of stellar mass loss, a trend which is not compensated by the decreasing velocity of the outflow at the outer edge of the galaxy. However, past this time the outflow velocity has decreased so much that the internal densities begin to rise, in spite of the continuing decrease in $\dot{M}_*$, and the density profile progressively tends to flatten. Correspondingly, the total amount of gas inside the galaxy, M_{gas}, reaches a minimum at $t \sim 5$ Gyr, precisely when the rate of mass loss from the galaxy $\dot{M}_{out} = 4\pi r_t^2 \rho(r_t) v(r_t)$ drops below the rate of injection of fresh gas, $\dot{M}_*$ (see Fig. 4). Up to $t \simeq 9$ Gyr the temperature distribution of the flow has not changed so much; it has simply decreased almost uniformly at all radii, as a result of the decreasing injection temperature. Inside the galaxy there is very little temperature gradient, basically thanks to the distributed supernova heating; but outside the galaxy the temperature radially drops as the escaping gas cools down in its quasi-adiabatic expansion (see Fig. 2).

At this point we distinguish between an early *wind* phase characterized by supersonic outward velocities, and a later *outflow* phase during which the gas still moves outward and leaves the galaxy but does so with a more and more subsonic velocity. The transition from the supersonic to the subsonic regime is rather smooth, however, and yet the outflow phase is inherently unstable, with a positive feed-back mechanism being set up. As more and more gas builds up inside the galaxy the central density rises, radiation losses become increasingly more important, a smaller fraction of the supernova heating is left to drive the flow, and in turn the flow deceleration causes a faster increase of the gas density. Inevitably, a moment comes when at the center the heating rate drops below the cooling rate, and a central cooling catastrophe suddenly reverts the direction of the flow in the inner region of the galaxy: the transition to an

TABLE 5

KG MODELS: DERIVED PARAMETERS

Model	$10^{21}\,\rho_{c*}$ (g cm^{-3})	r_{c*} (pc)	M_*/L_B ($M_\odot/L_\odot$)	$\chi(15)$	L_X (ergs s^{-1})	t_{cc} (Gyr)	M_{gas} ($10^9\,M_\odot$)	M_{sink} ($10^9\,M_\odot$)
K1	7.18	352	5.7	1.21	4.3×10^{41}	5.7	9.8	6.9
KRM	6.08	368	5.5	1.14	3.5×10^{41}	9.3	5.4	3.0
KRMa	6.08	368	5.5	1.14	1.6×10^{41}	5.7	5.7	4.0
KRMb	6.08	368	5.5	1.14	6.5×10^{41}	13.8	4.9	1.3
K2a	5.59	377	5.2	1.18	3.7×10^{41}	7.2	8.6	5.9
K2b	5.59	377	5.4	1.10	3.1×10^{41}	12.7	3.4	1.1
K2c	5.59	377	5.4	0.99	1.3×10^{38}	W	0.2	...
K2d	5.59	377	5.4	1.06	3.1×10^{39}	O	1.1	...
K3	5.12	386	5.4	1.06	4.3×10^{39}	O	1.1	...
K4	2.40	478	4.7	0.79	6.1×10^{37}	W	0.1	...
K5	1.83	696	5.6	1.21	8.2×10^{41}	7.2	19	10
K6a	1.31	764	5.1	1.14	7.9×10^{41}	13.5	10	2.3
K6b	1.31	764	5.3	1.06	3.2×10^{39}	O	2.8	...
K7	1.10	804	5.2	0.99	3.2×10^{38}	W	0.9	...

© American Astronomical Society • Provided by the NASA Astrophysics Data System

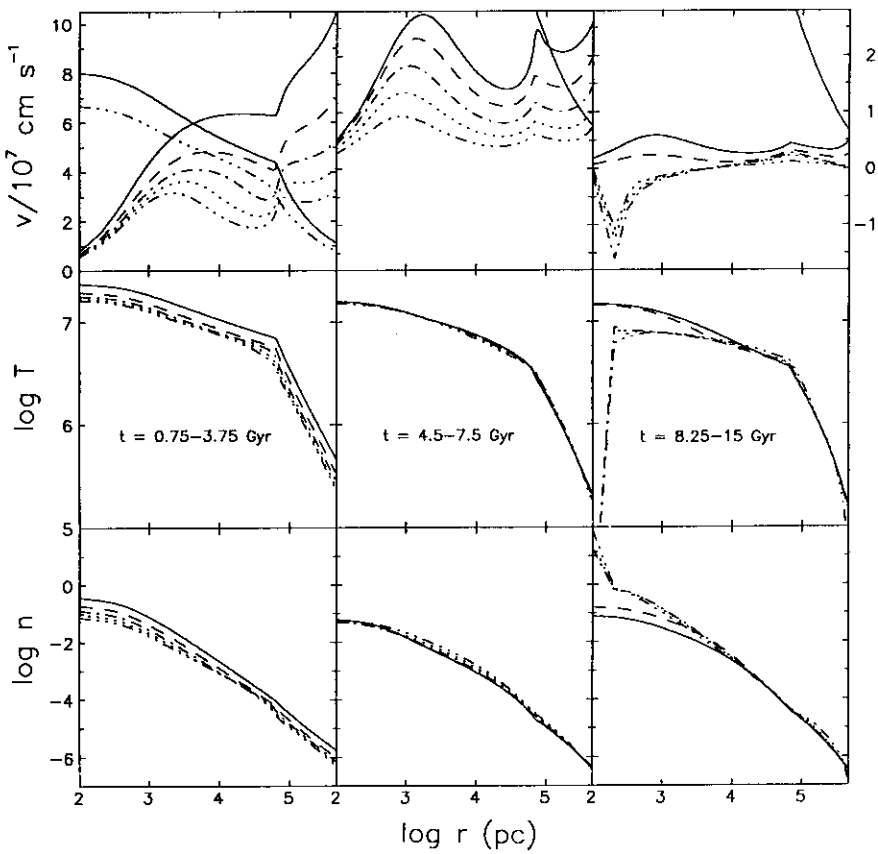

FIG. 2.—The gas velocity, temperature, and particle density for the KRM sequence as a function of the radial coordinate for a selection of representative times during the evolution of the flow. The various quantities are displayed at 0.75 Gyr intervals and are ordered according to the sequence of solid, dashed, dot-dashed, dotted, and three-dot-dashed lines. During the inflow phase, characterized by the presence of negative velocities, some of the models are omitted to avoid the overlap of many nearly identical lines. The sound velocity is also shown for two epochs in the first velocity panel (the monotonically decreasing lines) and for one epoch in the two other velocity panels, for which the right scale should be used.

inflow regime is virtually instantaneous. For the specific choice of parameters made for the KRM this happens at $t = 9.25$ Gyr, when negative infall velocities appear near the center and rapidly exceed ~ 100 km s^{-1} at a few 100 pc away from it. From this time on the inflowing material virtually disappears through the inner boundary located at $r = 100$ pc, just as in the case of cooling flow models without a distributed sink (see, e.g., Sarazin & White 1987; LM). It is worth noting that during the outflow phase the local cooling time (E/L) can become very short (i.e., $\sim 10^8$ yr), and yet the transition to the inflow regime takes a much longer time. This apparently unexpected behavior follows from the local heating exceeding cooling during the outflow phase, and therefore the gas keeps expanding.

As one can clearly recognize from the various panels in Figure 2, the central cooling catastrophe rapidly affects a substantial portion of the whole galaxy. Indeed, in a relatively short time scale ($\sim 10^8$ yr) the inner ~ 10 kpc are considerably affected, with an appreciable increase in density and decrease in temperature, coupled with a reversal in the flow velocity. It is the whole inner part of the gas component of the galaxy which suddenly shrinks. This is further illustrated in Figure 3, which shows the evolution of the stagnation point of the flow (where $v = 0$) from its first appearance at $t = 9.25$ Gyr onward. At the moment of the cooling catastrophe the stagnation radius r_{st} overshoots by a small amount the value it will later assume during the subsequent quasi-stationary inflow. During this phase the stagnation radius is very close to the effective radius r_e, while the stagnation mass $M_*(r_{st})$ is close to $M_*/2$, i.e., about one-half of the stellar mass loss flows in as an accelerated inflow, while the other half still flows out subsonically. As a result of the almost stationary stagnation point, the stellar mass loss inside r_{st} secularly decreases and so does the mass infall into the central sink. Note also that—apart from the innermost few 100 pc—the flow is still very subsonic, as it was during the previous outflow phase, i.e., there is little deviation from local hydrostatic equilibrium over most of the galaxy. Yet, exact hydrostatic equilibrium cannot be achieved due to the evolution of the source terms and to the presence of the central sink. Therefore, the actual flows during the inflow phase have several traits of resemblance with the pattern exhibited by cooling flow models but also several distinct characteristics. The similarities include quasi-hydrostaticity, flow pattern near the center, and total amount of hot gas within the galaxy. The main differences include the major deviations from steady state conditions, and the fact that the inflow is actually confined to only the inner part of the galaxy, while for $r \gtrsim r_e$ the subsonic outflow continues.

The evolution of the mass budget is shown in Figure 4. One can see that most of the stellar mass return ($\sim 10^{11} M_\odot$) is lost from the galaxy during the first ~ 2 Gyr, while it is in its wind phase. This is not a negligible fraction of the total stellar mass of the galaxy, and its effect on the early dynamical evolution of

© American Astronomical Society • Provided by the NASA Astrophysics Data System

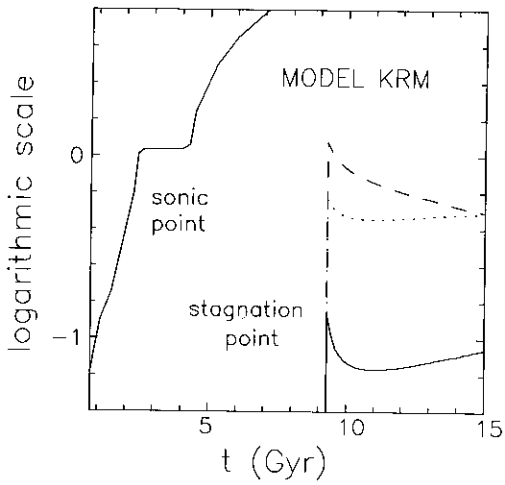

FIG. 3.—The time evolution of the sonic point and of the stagnation point for the KRM sequence. Both the sonic radius and the stagnation radius (*solid lines*) are in units of the tidal radius r_t. The fractional stellar mass coordinate of the stagnation point is also given (*dotted line*), i.e., $M_*(r_s)/M_*$, together with the instantaneous stellar mass loss inside the stagnation radius (*dashed line*), normalized to the total mass loss in the galaxy at $t = 15$ Gyr, i.e., $\alpha(t)M_* \simeq 0.75\ M_\odot\ \mathrm{yr}^{-1}$.

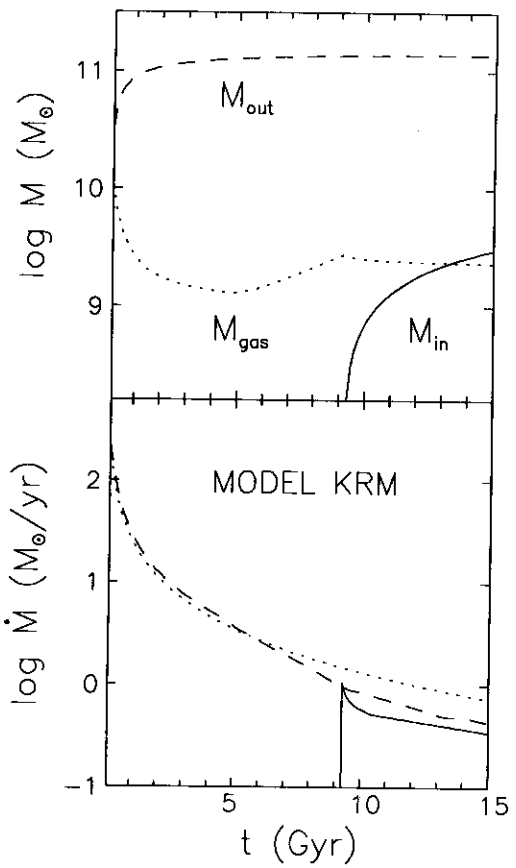

FIG. 4.—The time evolution of the mass budget of the gas flow of the KRM sequence. The upper panel shows the total mass of the hot gas inside the galaxy (M_{gas}), together with the total mass ejected from the galaxy and lost in the central sink, respectively M_{out} and M_{in}. The lower panel shows the time derivatives $\dot{M}_{out}$ and $\dot{M}_{in}$, together with the total rate of mass return $\dot{M}_*$.

the stellar component might have been relevant. Following LM we have neglected this effect, whose inclusion would have just complicated the models. On the other hand, our *single burst* models do not pretend to offer an accurate description of the very early evolution of elliptical galaxies, and soon after the first Gyr the mass loss from the galaxy becomes gravitationally insignificant and dynamical self-consistency is rapidly approached. The mass of hot gas inside the galaxy decreases during the wind phase, primarily as a consequence of the decreasing rate of mass return. However, the rate of mass loss from the galaxy $\dot{M}_{out}$ decreases faster than the rate of mass return and drops below it at the transition to the outflow phase. From this time on M_{gas} starts increasing, until the cooling catastrophe causes matter to suddenly slide into the central sink. During the inflow phase M_{gas} decreases, again as a result of the decreasing $\dot{M}_*$. Note also that in this specific case (as $r_{st} \simeq r_e$) the rate at which the gas leaves the galaxy through its outer edge is very close to the inflow rate through the central sink. The total amount of mass which has accumulated in the sink, i.e., the time integral of $\dot{M}_{in}$, is also shown in Figure 4; note that $\sim 10^9\ M_\odot$ of gas fall through the sink in the first $\sim 10^9$ yr past the central cooling catastrophe.

The evolution of the energy budget is shown in Figure 5. Besides L^+_{grav}, L^-_{grav}, L_{SN} and L_σ (see § 2.3 and § 2.4), also displayed are the total enthalpy flows through the inner and outer boundaries (respectively, L_{out} and L_{in}), together with the X-ray luminosity in the 0.5–4.5 Kev range, which represents the bulk of all radiative losses. Figure 5 shows that during the early supersonic wind phase much of the supernova energy input L_{SN} is used to extract the material out of the potential well and to accelerate it to its terminal velocity. So, during this phase $L_{SN} \simeq L^-_{grav} + L_{out}$, while $L_X \ll L_{SN}$, radiative losses represent only a minor term in the energy budget, and therefore have a negligible effect on the dynamics of the flow. As the flow decelerates and the galaxy enters the outflow phase, L_{out} decreases by about a factor of 10 below either L_{SN} or L^-_{grav}, and one has

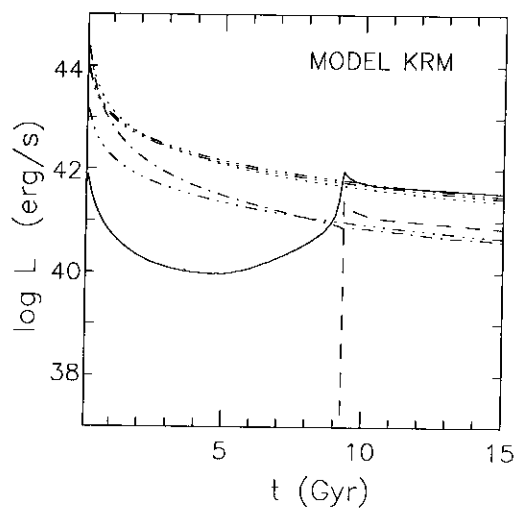

FIG. 5.—The time evolution of the energy budget of the gas flow of the KRM sequence. Displayed is the evolution of the X-ray luminosity L_X (*solid line*), together with L^+_{grav}, L^-_{grav}, and L_σ (*three-dot–dashed lines*, see text), and the enthalpy losses through the outer edge (L_{out}; *dot-dashed line*) and the central sink (L_{in}; *dashed line*).

© American Astronomical Society • Provided by the NASA Astrophysics Data System

$L_{SN} \sim L^{-}_{grav}$, i.e., virtually all the energy input is used to slowly lift the gas inside the potential well. Still, radiation losses are energetically negligible over most of the outflow phase, and only when the galaxy is already very close to its cooling catastrophe do they come to rapidly dominate its whole energetics, thus determining the transition to the inflow phase. This event temporally coincides with the sharp peak in L_X seen in Figure 5, certainly the most remarkable feature in the whole X-ray evolution of this model galaxy, as well as in the evolutionary history of its gas flow. During the peak, L_X somewhat exceeds $L^{+}_{grav} + L_{SN}$, as this short phase is inherently nonstationary, and heat which was stored in the course of the previous evolution is suddenly radiated away during the thermal catastrophe. Later, during the inflow phase $L_X \lesssim L^{+}_{grav} + L_{SN}$, as part of the supernova heating is still used to sustain the continuing outer outflow, while only a part of L^{+}_{grav} can be used to feed radiation losses, i.e., the fraction of it relative to the material which is actually flowing in. Note that subsequently to the development of the central inflow the estimated L_X includes the proper contribution from the enthalpy flow through the surface of maximum infall velocity. In the hypothesis of complete cooling of the falling material this energy has indeed to be radiated away.

As expected there is close similarity between the time evolution of L_X and M_{gas}, as cooling is proportional to the square of the density, while L^{+}_{grav}, L^{-}_{grav}, and L_σ evolve in a similar fashion being all proportional to $\alpha(t)$, and L_{SN} decreases faster than them (since $s > \sim 1.3$). Although the flow patterns can exhibit rather complex behaviors in terms of, e.g., supersonic versus subsonic velocities, or outflows versus inflows, still it is worth using simple definitions for the three main evolutionary phases experienced by the galactic gas flow. We define as the *wind* phase the one starting from the beginning of the evolution and ending when the relative minimum in M_{gas} and in L_X are reached. Yet, strictly speaking, a supersonic wind is present only during the earlier part of this phase. By the term *outflow* phase we designate the period of increasing M_{gas} and L_X which follows the wind phase and terminates with the central cooling catastrophe, at which time both M_{gas} and L_X reach a relative maximum. Finally, by the term *inflow* phase we designate the last stage starting with the cooling catastrophe, even if such an inflow is only partial.

Finally, there remains to present the evolution of the X-ray surface brightness profile $\Sigma_X(r)$ of this reference model. Figure 6 shows $\Sigma_X(r)$ for a number of interesting epochs during the three main phases, compared with the optical distribution. During the wind phase Σ_X is considerably more centrally peaked than the optical surface brightness, which results partly from the n^2 dependence of the emissivity, partly from the gas distribution being more concentrated than its stellar source, as v increases outward and degassing is therefore faster in the outer part of the galaxy. However, as the flow decelerates and turns into a slow outflow large amounts of hot material begin to pile up, and Σ_X exhibits a profile which is increasingly broader than the optical distribution. This tendency continues all the way through the outflow phase and suddenly reverts at the transition to the inflow phase, which is characterized by a very peaked, almost stationary X-ray surface brightness profile. Note the similarity of the present Σ_X profiles during the inflow phase, with those presented by LM in their Figure 11. Following LM, in our Figure 6 the central spike corresponding to the enthalpy loss in the sink is not shown for the inflow models. In conclusion, the three evolutionary phases are clearly characterized by vastly different combinations of the L_X/L_B and $\Sigma_X(r)/\Sigma_B(r)$ ratios, a property which can allow to observationally identify the evolutionary phase of an X-ray galaxy.

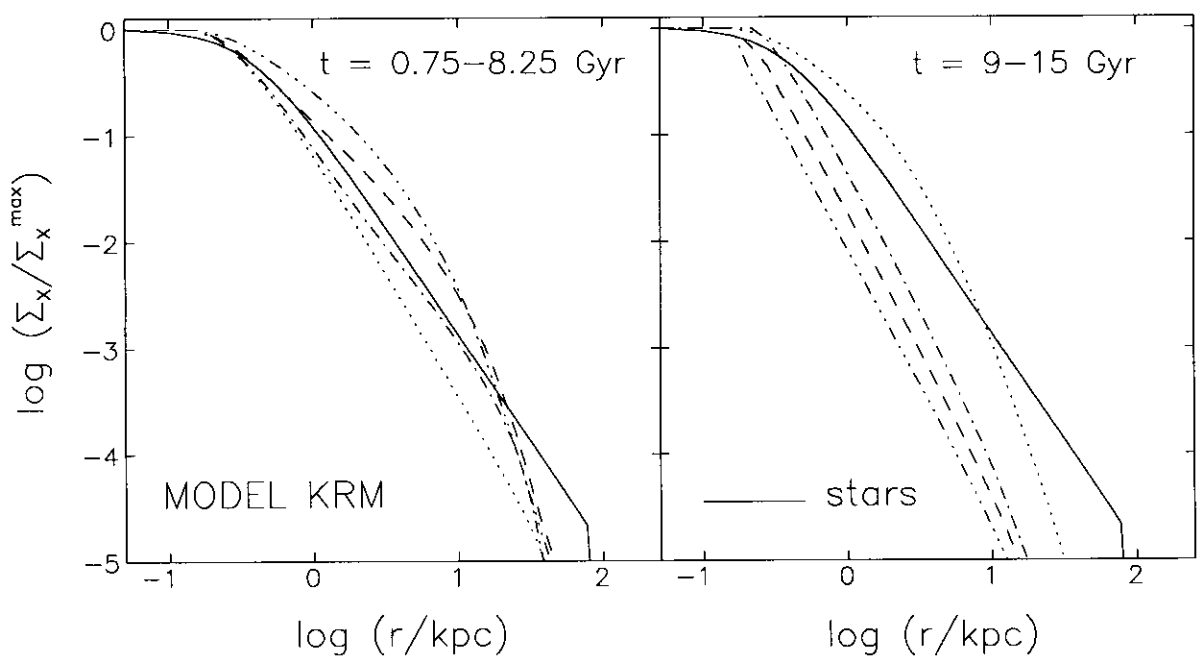

FIG. 6.—The evolution of the X-ray surface brightness profile (for the 0.5–4.5 keV range) for a selection of representative models during the various evolutionary phases. In the left panel models in the wind phase (*dotted line*) and outflow phase (*other lines*) are displayed. In the right panel a model toward the end of the outflow phase is shown (*dotted line*), together with a few models in their inflow phase (*other lines*). The time order of line types is the following: dotted, dot-dashed, dashed, and three-dot–dashed. The possible contribution from the enthalpy flow into the central sink is ignored. The optical surface brightness profile is also shown for reference (*solid line*).

© American Astronomical Society • Provided by the NASA Astrophysics Data System

4.2. *Exploring the Parameter Space*

So many parameters are required to fully determine a model galaxy that testing each possible combination of them would be a rather cumbersome matter. We therefore explore a few such combinations, and following the arguments presented in § 2.4, we first focus on those implying present χ values about unity for medium-luminosity galaxies ($L_B \simeq 5 \times 10^{10}\ L_\odot$). Indeed, for χ values much different from unity such galaxies would now be in either a wind or an inflow phase, and so either too faint or too bright X-ray emitters. Equation (16) thus restricts the possible combinations of ϑ_{SN} and R. We explore only one value of the other supernova parameter s, adopting $s = 1.5$ for all our simulations. Indeed, for $s \lesssim 1.3$ most galaxies would have experienced massive early inflows such as in LM models, while we want to avoid excessive accumulation of cooled matter in the core of the galaxies. On the other hand, values of s much larger than 1.3 would imply a very high initial SN rate, and then a possible overproduction of iron during early galactic evolution. We are therefore left with a fairly narrow range of allowed s values, around 1.4–1.5, which justifies our choice (see § 7.1).

For all the computed KG models Table 4 lists the values of their input parameters, while Table 5 lists a number of derived structural parameters, i.e., r_{c*}, ρ_{*0}, M_*/L_B, and $\chi(15)$, together with the present X-ray luminosity L_X, the present amount of gas within the galaxy M_{gas}, the amount of matter which has passed through the central sink M_{sink}, and the time at which the cooling catastrophe takes place (t_{cc}), as they all result from the hydrodynamical calculations. For those models which at $t = 15$ Gyr have not yet suffered their cooling catastrophe, instead of t_{cc} Table 5 indicates the present evolutionary stage of the galaxy (W = wind, O = outflow). The X-ray evolution of all the $L_B = 5 \times 10^{10}\ L_\odot$ models in Table 5 is shown in Figure 7, with the exceptions of KRMa and KRMb which will be commented later. Models K1, K2b, K3, and K4 differ only for their central velocity dispersion σ_*. As the depth of the potential well and L_{grav}^- are both proportional to σ_*^2, the larger the σ_*, the sooner the model galaxies experience their cooling catastrophe and the associated X-ray brightening. So, while at $t = 15$ Gyr models K1 and K2b have already experienced their transition to the inflow phase, model K3 is still in its outflow phase, and model K4 is in its wind phase. All other parameters being fixed, we therefore expect a very high sensitivity of L_X to variations of σ_* in the range $\sim$240–265 km s^{-1}, with L_X increasing from $\sim 10^{38}$ to over 10^{41} ergs s^{-1}.

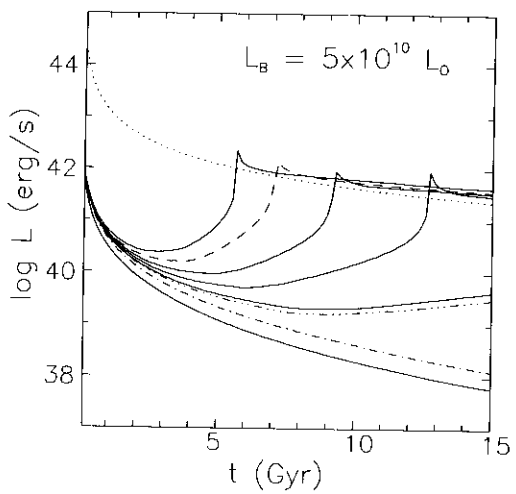

FIG. 7.—The X-ray evolution of various models listed in Table 4. With the solid lines are represented the sequences K1, KRM, K2b, K3, and K4 which differ only for their value of the central velocity dispersion σ_*. They can be identified thanks to the value of t_{cc} and/or L_X given in Table 5. Also shown is the X-ray evolution of the sequences K2a (*dashed line*), K2c (*dot-dashed line*), and K2d (*three-dot–dashed line*).

However, models in the critical range of σ_*'s will also be very sensitive to changes in every other parameter, as illustrated by models K2a, K2c, and K2d. Model K2a is identical to K2b apart from the value of δ. By reducing δ the KG models are truncated at a smaller r_t, but $\rho_*(r)$ remains unaffected inside the new tidal radius. So the new M_* is decreased by the mass which has been truncated away ($\sim$4%), while the total rate of mass return stays the same as it depends only on L_B. Moreover, the reduction in the volume of the galaxy, while keeping the same R, forces more dark matter at smaller radii, thus deepening the potential well, and increasing L_{grav}^- and χ (see Table 5). So the reduction of the parameter δ means more than just a truncation of the galaxy at a smaller r_t and mainly mimics the effect of a certain shrinkage of the dark matter distribution, with the parameter β increasing from 4.5 to 4.9. As a net effect, χ increases and both the wind-outflow and outflow-inflow transitions are considerably anticipated, the latter one from $\sim$13 to $\sim$7 Gyr. Although the final configurations and X-ray luminosities do not differ significantly, the evolutionary histories of K2a and K2b sequences are clearly rather different.

The effect of the distribution of dark matter is further illustrated by the comparison of sequences K2b, K2c, and K2d, which differ only for the value of γ, i.e., for the central density of dark matter. Reducing γ has the effect of spreading out the dark matter at larger radii (while keeping its total mass the same); thus L_{grav}^- and χ decrease, and the transition to the inflow phase is dramatically delayed: model K2c is indeed still in its wind phase at $t = 15$ Gyr, with small M_{gas} and low L_X.

Sequences KRMa and KRMb illustrate what happens when both the supernova heating and the confining dark matter are decreased or increased while keeping χ the same. This is achieved by, respectively, decreasing and increasing the parameters ϑ_{SN} and R, and using equations (15) and (16) to ensure the near constancy of χ. Also the parameter β has been kept the same as in the KRM, so as to maintain a similar distribution of the dark matter. So, the decrease in the total amount of dark matter is accomplished by reducing its central density, i.e., the parameter γ, see Table 4. With these choices the models KRM, KRMa, and KRMb should be *energetically equivalent*, at least on a global scale. Figure 8 shows the X-ray evolution of the three models. The duration of the wind phase is nearly the same in the three cases, but the duration of the outflow phase is much different, with t_{cc} increasing from $\sim$5.7 to $\sim$13.8 Gyr between sequences KRMa and KRMb. Indeed, the energetic equivalence of the three models does not ensure perfect identity in the behavior of the flows. For example, going from KRM to KRMa the reduced SN rate causes a reduction in the flow velocity in the central regions (where the concomitant reduction of the dark matter does not have a direct local impact), degassing is slower, and the cooling catastrophe is anticipated. Conversely, as the gas in the central regions becomes more bound, the opposite happens to the outer regions of the galaxy, and faster degassing is promoted. So, by reducing the SN rate while keeping χ the same the flow

© American Astronomical Society • Provided by the NASA Astrophysics Data System

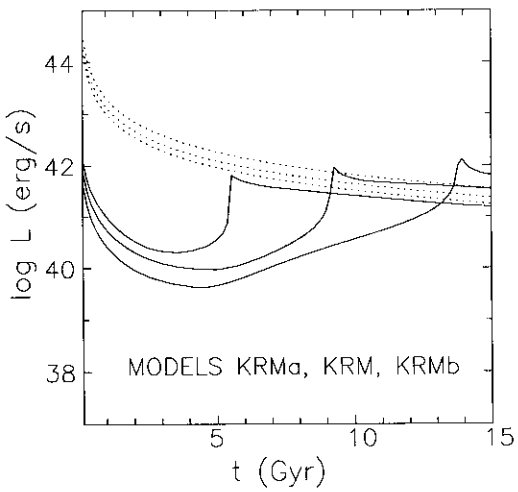

FIG. 8.—The X-ray evolution for the three *equivalent* sequences KRMa, KRM, and KRMb, which can be identified by their value of t_{cc} in Table 5. Also reported is the evolution of the SN luminosity L_{SN} for the three sequences (*dotted lines*).

develops a *core-envelope* structure, with a fairly small central inflow coupled with an extended outer outflow. The opposite trend is realized by increasing the SN rate, as this facilitates central degassing and delays the onset of the inflow phase. These trends are further illustrated by the behavior of the stagnation point in the three models, shown in Figure 9. Note that the larger final X-ray luminosity in sequence KRMb, compared to KRM or KRMa, is a combined consequence of the higher L_{SN} and of the larger stagnation radius.

We now comment on models with $L_B = 10^{11}\ L_\odot$ (sequences K5–K7). Note that χ is independent of L_B (see eqn. [16]), and therefore models which differ only for the value of L_B are automatically *equivalent*. Note also that the K5 model experiences its cooling catastrophe ~ 1.5 Gyr after its equivalent K1. This is due to model K5 having a lower central density (see Table 5),

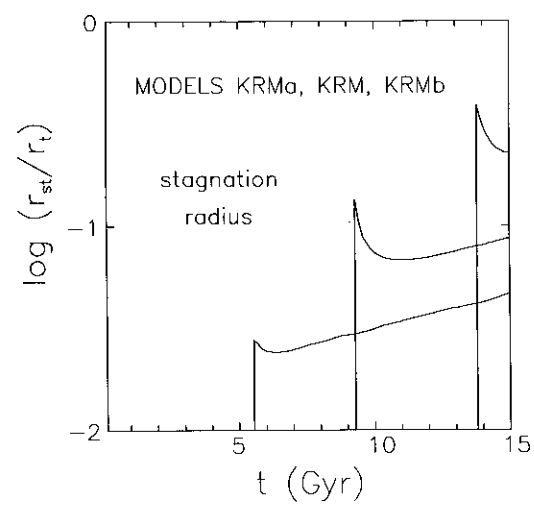

FIG. 9.—The evolution of the stagnation radius r_{st} (in units of the tidal radius r_t), for the three *equivalent* sequences KRMa, KRM, and KRMb. Note that the core of the galaxies becomes more bound and their envelope more unbound when decreasing both the supernova rate and the amount of dark matter (while keeping χ constant).

a consequence of having forced KG models to lie on the FP. From equation (1), increasing L_B while keeping the same σ_* forces r_e to increase and one gets bigger, thus lower density galaxies. With lower stellar densities the resulting gas densities are also lower, radiative losses are reduced, and then the cooling catastrophe delayed. Similar considerations hold for the sequences KRM and K6a. At first sight this seems to indicate that increasing L_B would tend to favor winds and outflows over inflows, and then lower X-ray luminosities, contrary to the trend shown in Figure 1. However, not all σ_*'s are equally probable at different L_B's, but the average σ_* increases with increasing L_B (as demanded by the Faber-Jackson relation), and this effect will tend to dominate in a large sample of galaxies.

In summary, an inspection of Table 5 reveals that, in general, models with $\chi \gtrsim 1.10$ tend to be in the inflow phase at $t = 15$ Gyr, those with $1.0 \lesssim \chi \lesssim 1.10$ tend to be in the outflow phase, and those with $\chi \lesssim 1.0$ in the wind phase, as expected. For $\chi \lesssim 0.9$ the flow is still supersonic over a large fraction of the galactic body. From all the above discussion we conclude that any of the parameters is able to vary the time t_{cc} at which the inflow phase begins; there exists, however, a huge number of combinations in which two or more parameters can be tuned in such a way to leave t_{cc} unchanged. Conversely, for $\chi \approx 1$ models any small variation in the input parameters can produce large variations of t_{cc}, and therefore in L_X. As we have argued in Paper I, this flexibility makes the present class of models very attractive in the context of the observed spread in the $L_X - L_B$ relation, which is naturally accounted for in terms of modest dispersions in every one of the relevant parameters which must certainly exist among real galaxies.

In concluding this section, we emphasize that this extreme sensitivity of L_X on σ_* is the key characteristic of our model galaxies and can therefore account for the very steep $L_X - \sigma_*$ correlation, as well as for the correlation of L_X with L_B; see Figure 1. As already mentioned, the larger the σ_* the deeper the potential well (i.e., the larger the binding energy per unit mass), the harder for the gas to leave the galaxy, and the earlier in the evolution the transition to the X-ray bright evolutionary phases. In turn, the Faber-Jackson relation ensures that—on average—the brighter the optical luminosity of the galaxy, the larger σ_*, and therefore the larger also the X-ray luminosity. The situation is fairly similar to the case of early galactic wind models for the chemical evolution of elliptical galaxies (e.g., Larson 1974; Arimoto & Yoshii 1987), according to which in the more massive (and now brighter) galaxies the deeper potential well ensures star formation and metal enrichment to proceed further before being discontinued by the development of a wind, thus establishing the observed metallicity-luminosity correlation. In essence, we propose that *both the $L_X - L_B$ correlation, and the metallicity-luminosity correlation, are two manifestations of the same underlying cause, i.e., of the fact that optically brighter galaxies are also gravitationally more tightly bound, as dictated by the Faber-Jackson relation.* The presence of metallicity gradients in ellipticals adds further support to this scenario (see Franx & Illingworth 1990).

5. THE dVG EVOLUTIONARY SEQUENCES

The main difference between KG and dVG models is in their nuclear regions, with dVG models being characterized by much higher stellar densities. This has two distinct effects on the gas flows: (1) central gas densities are higher in dVG

© American Astronomical Society • Provided by the NASA Astrophysics Data System

TABLE 6

dVG MODELS: INPUT PARAMETERS

Model	L_B ($10^{11} L_\odot$)	σ_* (km s^{-1})	R	β
dVRM	0.5	275	9	0.176
dV1	0.5	280	12	0.375
dV2	0.5	270	12	0.375
dV3	0.5	265	12	0.375
dV4	0.5	220	12	0.375
dV5	0.5	280	11	0.5
dV6	0.5	300	9	0.375

NOTE.—For all models $\delta = r_t/r_e = 15$.

models, and therefore radiative losses are locally more severe, and (2) the potential well presents a deeper minimum of small spatial extension, which makes somewhat harder to extract the gas from the innermost few 100 pc, compared to KG models. Both effects actually cooperate to this end, as the extra radiative losses subtract energy otherwise available to lift the gas.

To exemplify the evolution of the gas flow in a dVG model we adopt as *reference model* (dVRM) a galaxy characterized by the set of input parameters given in Table 6 and derived parameters given in Table 7. As all the models presented in this section, the dVRM is characterized by a nuclear radius $r_n = 100$ pc, while the SN parameters are the same as for the KRM. It is worth mentioning that this specific model does not lie on the FP as defined by equation (1), although it is not far from it (for the same σ_* and r_e this equation would imply $L_B \simeq 8 \times 10^{10} L_\odot$, rather than $5 \times 10^{10} L_\odot$). However, some properties of this specific model have been already presented elsewhere (D'Ercole et al. 1990), and we would like to complete its description here. All other dVG models in Table 6 do actually lie on the FP. Figure 10 shows the behavior of the flow velocity for a number of relevant epochs along the evolution of the dVRM sequence. The main difference with respect to the analogous Figure 2 is the presence of a small *mini-inflow* only ~ 300 pc in size, near the center of the galaxy. This is due to the very centrally peaked concentration of matter, which favors the early, localized cooling catastrophe. Therefore, for most of the time the model presents this small mini-inflow coupled to an outer wind or outflow. The global, much more extended cooling catastrophe takes place later, at $t = 10.2$ Gyr, and we can still speak of a wind, an outflow, and an inflow phase just as for KG sequences, with the proviso that a mini-inflow is present during most of the wind and outflow phases.

Figure 11 shows the behavior of the stagnation point, which soon appears at $t \simeq 0.5$ Gyr. The stagnation point associated to the mini-inflow remains nearly stationary during most of the wind and outflow phases, while the mass loss inside it decreases as $\sim t^{-1.3}$, following the decrease in $\alpha(t)$, reaching a minimum of less than $\sim 10^{-2} M_\odot$ yr^{-1}. Then the stagnation point starts accelerating outward, as the global cooling catastrophe is approached. Figure 12 shows that the presence of a mini-inflow causes some $10^9 M_\odot$ of gas to sink near the center early in the evolution of the flow. Apart from mini-inflow effects, the behavior of the other terms in the mass budget is similar to that exhibited by KG sequences, and the same comments apply. Notice that $M_{\rm gas}$ does not decrease in this case during the inflow phase, a result of the faster migration of the stagnation point, compared to the KRM sequence.

The X-ray evolution of the dVRM is shown in Figure 13, together with that of all the dVG sequences in Table 6. The overall evolution is much similar to the case of KG sequences, in spite of the presence of the mini-inflows. Subtle differences, however, exist. The case is illustrated by the two sequences dVRM and dV4 for which Figure 13 shows also the evolution of L_X including the mini-inflow contribution (i.e., the enthalpy loss in the sink). This contribution can be important during the wind phase and becomes progressively marginal during the outflow phase, as the X-ray emission from the accumulating, diffused gas increases. Also, to the onset of the mini-inflow is due the modest bump in L_X which is visible at early times for the sequences dVRM and dV4. In the case of this latter sequence, it is interesting to notice that the mini-inflow luminosity dominates over the diffused contribution, from the onset of the mini-inflow all the way to the present. We conclude that if mini-inflows exist, they should manifest themselves as almost pointlike central X-ray sources, with $L_X \simeq$ few times 10^{38} ergs s^{-1}. Much brighter point sources would of course be present in inflow models, characterized by a much larger mass infall.

Finally, we briefly comment on the influence of the adopted central truncation of the (otherwise singular) de Vaucouleurs' distribution. We find that for the dVRM an increase of the nuclear radius r_n from 100 to 200 pc (thus decreasing the central density) has the effect of significantly delaying the overall cooling catastrophe, from ~ 10 to slightly over 15 Gyr (D'Ercole et al. 1990). This illustrates that also the detailed mass distribution near the center can have a nonnegligible effect on the overall characteristics of the evolving gas flows, thus adding further variance to an already rich plethora of possible evolutionary histories.

6. EFFECTS OF THE ENVIRONMENT

All the models presented so far refer to the evolution of isolated galaxies. Actually, real galaxies continuously interact with their environment, e.g., with the intracluster medium through which they plough, with neighboring galaxies during

TABLE 7

dVG MODELS: DERIVED PARAMETERS

Model	$10^{20} \rho_{c_*}$ (g cm^{-3})	r_e (pc)	M_*/L_B ($M_\odot/L_\odot$)	χ (13)	L_X (ergs s^{-1})	t_{cc} (Gyr)	$M_{\rm gas}$ ($10^9 M_\odot$)	$M_{\rm sink}$ ($10^9 M_\odot$)
dVRM	3.05	7690	9.7	1.19	5.0×10^{41}	10.2	12	3.5
dV1	3.57	4219	4.8	1.20	1.0×10^{42}	9.3	20	11
dV2	3.24	4420	4.7	1.13	5.6×10^{41}	O	8.1	2.4
dV3	3.09	4526	4.6	1.09	2.7×10^{40}	O	5.5	2.2
dV4	1.87	5739	4.0	0.79	3.3×10^{38}	W	1.6	1.5
dV5	3.57	4219	4.8	1.09	1.5×10^{40}	O	4.8	2.7
dV6	4.29	3864	5.0	1.09	1.8×10^{40}	O	5.3	3.3

© American Astronomical Society • Provided by the NASA Astrophysics Data System

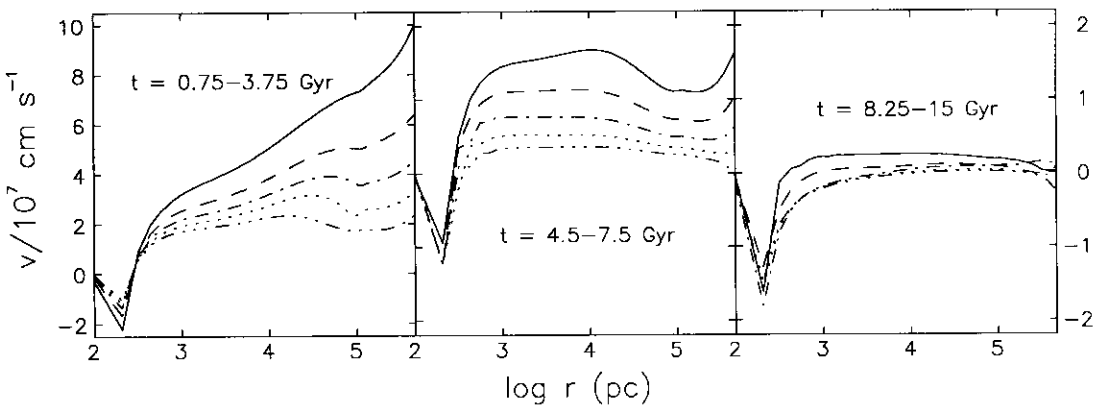

FIG. 10.—The gas velocity as a function of the radial coordinate is given for a selection of representative epochs during the evolution of the flow in the dVRM sequence. The three panels refer to the time intervals 0.75–3.75 Gyr, 4.5–7.5 Gyr, and 8.25–15 Gyr, respectively. For other details, see Fig. 2 caption.

tidal encounters, or even suffering more violent phenomena such as close collisions or merging events. Although the modeling of hot-gas flows during events of this kind is beyond the scope of the present investigation, still a few considerations are in order.

6.1. *Intracluster Gas Pressure and Ram Pressure Effects*

The proper gasdynamical study of a galaxy moving through the intergalactic medium needs at least a two-dimensional treatment. Our code being one-dimensional, we modeled the interaction with the external medium in the simplest possible way: we assumed our model galaxy to be surrounded by an infinitely extended atmosphere with a pressure $P_{ext} = 2 \times 10^3$ cm^{-3} K, typical of a small X-ray cluster (see, e.g., Vedder, Trester, & Canizares 1988). As a test galaxy we assumed a dVG model with $\sigma_* = 215$ km s^{-1}, the other parameters being the same of the dVRM. With this choice one has $\chi = 0.79$ at $t = 15$ Gyr, and the evolutionary models give a galaxy still in its wind phase at the present epoch, when $P_{ext} = 0$ is assumed. Contrary to the case with $P_{ext} = 0$, in the sequence with $P_{ext} \neq 0$ the containing effect of the outer pressure soon causes the wind to stall into a subsonic outflow (at $t \simeq 1$ Gyr), and the transition to the inflow phase takes place at $t \simeq 6$ Gyr. As a net result the final X-ray luminosity is $\sim 10^{42}$ ergs s^{-1}, as opposed to only $\sim 10^{38}$ ergs s^{-1}. Moreover, during the inflow phase $L_X \simeq 2$ $(L_{SN} + L^+_{grav})$, i.e., about twice what expected in the case of an isolated inflow galaxy. A detailed inspection to the evolution of the flow reveals the origin of this phenomenon. Initially the dynamics of the gas is not affected by the presence of the outer pressure and behaves as in the isolated models; in particular,

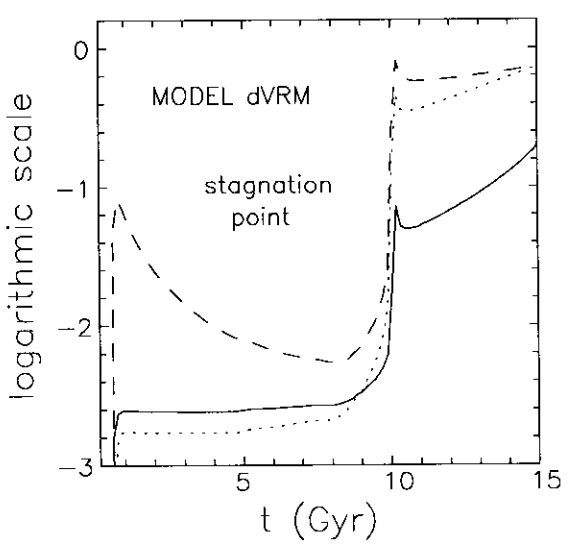

FIG. 11.—The time evolution of the stagnation point for the dVRM sequence. Also see Fig. 3 caption.

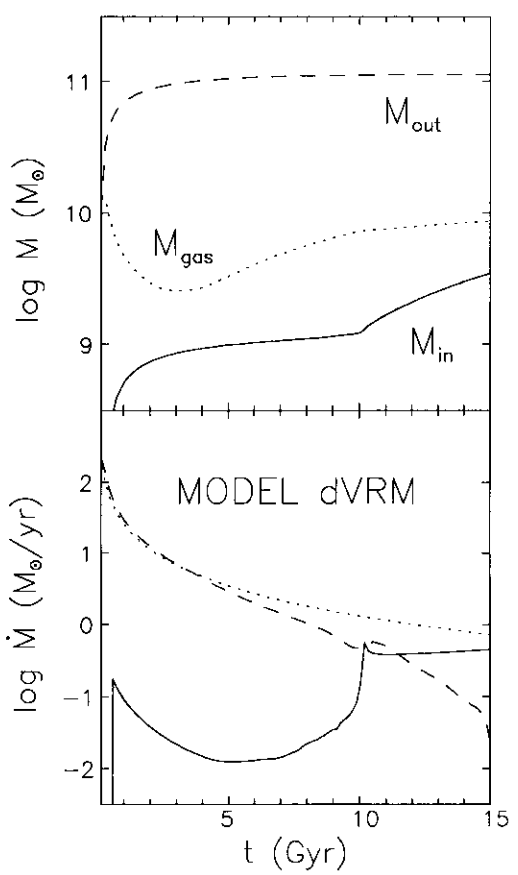

FIG. 12.—The time evolution of the mass budget of the gas flow for the dVRM sequence. Also see Fig. 4 caption.

© American Astronomical Society • Provided by the NASA Astrophysics Data System

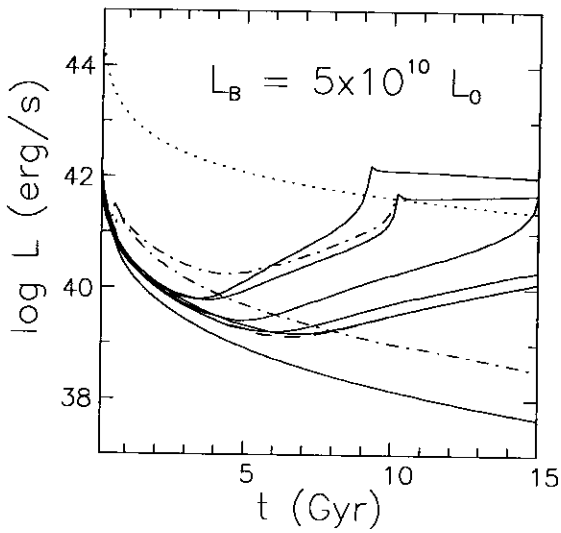

FIG. 13.—The X-ray evolution of dVG sequences listed in Table 6, which can be identified by the value of t_{cc} and/or L_X given in Table 7. The dashed line represents sequence dV5. For sequences dVRM and dV4 the dot-dashed lines represent the L_X evolution when including the contribution of the mini-inflow. The bump at $t \simeq 0.5$ Gyr is caused by the onset of the mini-inflow. Note also that at $t = 15$ Gyr the model dV2 is caught right at the moment of its global cooling catastrophe. The dotted line represents L_{SN}.

the velocity increases with radius while the central density decreases. At the outer edge of the galaxy, however, the velocity drops and the gas accumulates. So the gas is *not* lost by the galaxy but remains confined to its surroundings, while the density gradient becomes shallower. When the central density has sufficiently increased the usual inflow is triggered, and all the gas previously pushed outward falls back through the potential well, thus releasing more energy than the stationary L^{+}_{grav}. The extracontribution to L_X does *not* come either from the external pressure work or from the infall of intracluster gas: it is instead the delayed infall of the stellar mass loss material to cause the excess X-ray luminosity.

For the same model galaxy we have also run a third evolutionary sequence, keeping the same outer pressure but with $R = 4.5$, i.e., with half the amount of dark matter. As a result the galaxy is still in the outflow phase at the present epoch, although about to flip to the inflow regime. For the X-ray evolution of these three sequences see D'Ercole et al. (1990). These examples effectively illustrate the relative roles of dark matter and outer pressure. As expected, the outer pressure simulates the presence of a massive dark halo, a similarity also exhibited by steady cooling flow models (Sarazin & White 1987; Vedder, Trester, & Canizares 1988).

Certainly, also the case of a galaxy permanently at rest with respect to the ambient medium is a very idealized one: galaxies move at high velocity within clusters and groups, thus experiencing a ram pressure, a problem already investigated by several authors. Takeda, Nulsen & Fabian (1984) find that a large fraction of the accumulated interstellar gas is pushed out in a single blob on each passage through a dense cluster core, giving rise to a periodic behavior in the interstellar gas content of the galaxy. In all studied cases the maximum gas mass accumulated does not exceed $10^9\ M_\odot$, insufficient to account for the brightest X-ray galaxies in the CFT sample. However, such galaxies belong to rather small groups, where ram pressure is much smaller than at the center of rich clusters. Gaetz, Salpeter, & Shaviv (1987) find that gas is ablated from the outer portions of the galaxy but is retained in the central region of a cooling flow model. Still, the mass of the interstellar gas is less than $10^9\ M_\odot$.

The above results cannot be directly applied to our case, given the different treatment of the stellar distributions and of the source terms. New two-dimensional calculations are therefore needed to investigate how our models interact with the ambient medium. The most interesting case is that of galaxies in their outflow phase. Indeed, ram pressure effects on an outflow galaxy are particularly difficult to predict, as such a phase is highly thermally unstable, and the interaction with the ambient gas can either anticipate the central cooling catastrophe and the transition to the inflow regime, or totally strip the galaxy depending on the details of the interactions. Subsonic outflow configurations are in fact rather fragile and may evolve either way toward inflows or winds. While the outer parts of the X-ray coronal gas are certainly ablated, what happens to the inner core is less clear, but transitions from outflows to partial winds appear possible, when ram pressure forces compress the core of a subsonic flow, while stripping the envelope away. As far as the X-ray luminosity is concerned, ram pressure can either increase or decrease L_X, depending on whether or not a core inflow is triggered.

Although purely global arguments are insufficient to fully predict the characteristics of the flows, still they may be useful for a quick evaluation of the relative importance of the various terms affecting such flows. With this limitation in mind, we introduce the ram pressure *luminosity* as the work done per unit time by ram forces on the X-ray gas:

$$L_{ram} \simeq n m_p v^3 \pi r_{ge}^2 \simeq 10^{40}\left(\frac{n}{10^{-5}}\right)\left(\frac{v}{1000}\right)^3\left(\frac{r_{ge}}{5000}\right)^2 \text{ergs s}^{-1}, \quad (21)$$

where n is the particle density of the intracluster medium (in cm^{-3}), v is the velocity of the galaxy with respect to this medium (in km s^{-1}), and r_{ge} is an effective radius (in pc) for the gas distribution within the galaxy. The power L_{ram} acts in the sense of extracting gas from the galaxy, and it makes sense to compare it to the power L^{-}_{grav} required to steadily extract the gas. More than this, we can attempt a generalization of equation (16) to include the ram luminosity, i.e.,

$$\chi(t) = \frac{L^{-}_{grav}(t)}{L_\sigma(t) + L_{SN}(t) + L_{ram}(t)}, \quad (22)$$

and total stripping may be favored when L_{ram} competes with L_{SN} in keeping χ below unity. In optically bright galaxies one typically has $L_{SN} \simeq L^{-}_{grav} \simeq 10^{42}$ ergs s^{-1}, and equation (21) indicates that ram pressure should not be important in small clusters and groups but may become the dominant factor in rich clusters (see also Takeda et al. 1980).

While we avoid overinterpreting equation (22), we note that supernovae and ram pressure can efficiently cooperate in keeping low gas densities inside galaxies, with SN-induced outflows increasing the effective radius r_{ge}, and therefore helping ram pressure to complete the gas removal. In turn, ram pressure degassing in the outer regions (which have a larger cross section) helps maintaining an outflow, and a runaway evaporation can result, in particular when a galaxy happens to cross the core of a cluster. Again, the particular history of each

© American Astronomical Society • Provided by the NASA Astrophysics Data System

cluster galaxy will add further diversities to the evolution of their gas flows and X-ray luminosities. This indicates that an evolutionary approach is required to properly treat the ram pressure effects.

Apart from the frequently referred case of the M86 plume, there is little additional evidence of ram pressure effects among *Einstein* X-ray galaxies. However, Canizares (1988) reports indications of a systematic X-ray underluminosity of ellipticals in the rich Coma cluster, compared to closer ellipticals such as those in Virgo (which is a looser cluster), and attributes the difference to more effective ram-pressure stripping in Coma. Sarazin & White (1990) suggest that galaxy-to-galaxy differences in environment (and then in ram pressure) may account for the dispersion in X-ray luminosity seen in Figure 1, and find a correlation between L_X and the local density of galaxies. Whether this is due to ram pressure or to tidal stripping of the dark matter halo (which both would tend to decrease the effective χ) remains to be established but certainly what ultimately matters is the relative size of the various terms appearing in equation (22).

So far we have neglected heat conduction in all our models; the temperature distribution is indeed almost flat (see Fig. 2) and conduction is not expected to be important (see also LM). However, when a hot external medium is considered, large temperature gradients are to be expected between the gas inside the galaxy ($T \simeq 10^7$ K) and the much hotter intracluster gas (up to $\sim 10^8$ K). We have correspondingly allowed for electron conduction in our previous model with outer pressure and have adopted $n_e = 10^{-5}$ cm^{-3} and $T_e = 10^8$ K as representative for the electron density and temperature in a rich cluster such as Coma. If thermal conduction is not suppressed by magnetic fields, heat is then expected to flow into the galaxy. The corresponding heat transfer into our model galaxy turns out to be very high (up to $\sim 10^{44}$ ergs s^{-1}), much larger than any other energy budget of the galaxy. We have run an evolutionary sequence which includes such an effect and, as expected, thermal conduction dominates to the extent that no significant amount of gas accumulates inside the galaxy, i.e., we have a persistent wind powered by thermal conduction. Clearly, if the heat conduction is not efficiently suppressed evaporation can hardly be avoided (Cowie & Songaila 1977). In this connection, our numerical simulation indicates that the suppression of the heat conduction (by magnetic fields) should be virtually complete if the existence of powerful X-ray ellipticals is to be preserved in rich clusters. We also note that very large heat transfer rates would still be predicted also for intracluster temperatures considerably lower than the fairly high value adopted in our numerical simulation.

6.2. *Encounters with Other Galaxies*

There is currently wide interest in the idea of elliptical galaxies being formed by dissipationless merging of smaller stellar systems, although early objections (Ostriker 1980) still await for a satisfactory answer, and fresh data on color and metallicity gradients (e.g., Franx & Illingworth 1990; Peletier 1989) lend support to the notion of dissipational star formation playing a leading role in the formation of ellipticals and bulges. Our models are clearly inadequate to describe late merging events, but may still represent an acceptable simplification for those cases in which the bulk of merging took place a long time ago. Late merging events may, however, occur, and it seems legitimate to speculate about their possible effects on the X-ray gas. Again, the most interesting evolutionary phase is the outflow phase. A relatively wide tidal encounter could indeed resuscitate a supersonic wind by either stripping part of the dark matter halo, or by temporarily reducing the effective $L_{\rm grav}^{-}$. In both cases the net result would be a decrease of L_X. On the contrary, in the case of a merging with a smaller galaxy the resulting deepening of the potential well could anticipate the transition to the inflow regime and produce a major X-ray brightening. In this scenario the boxiness-L_X correlation mentioned in § 1 (if it really exists) may perhaps be accounted for by a late merging event causing at once the boxy isophotal distortion and the transition to the inflow regime. Still in the case of merging, one could further distinguish between gas-rich and gas-poor captured galaxies (e.g., dwarf ellipticals vs. dwarf irregulars), with the cold gas of the latter ones perhaps acting as a seed for the cooling catastrophe, or promoting optical emissions in the course of its evaporation (see Sparks & Macchetto 1990). In any event, it is the mere existence of a prolonged outflow phase which tends to amplify any galaxy-to-galaxy difference, either intrinsic or environmental. Alternatively, the correlation may arise from the $L_{\rm grav}^{-}/L_B$ ratio being systematically smaller in galaxies which are in part rotationally supported, compared to purely pressure-supported systems. We tend to favor this interpretation, although a quantitative approach is beyond the reach of our spherically symmetric models. Indeed, we note that among the four disklike galaxies in Figure 1 with $L_B \simeq 10^{11}$, NGC 4697, 4382, and 6876 exhibit a rather low σ_* (respectively 165, 185, and 231 km s^{-1}) and a low X-ray luminosity, while $\sigma_* = 337$ km s^{-1} in the X-ray bright galaxy NGC 7619. It seems reasonable to argue that galaxies with small σ_* have also a somewhat shallower potential well (even if partly rotationally supported), and therefore lower χ values compared to galaxies with the same L_B but larger σ_*.

7. DISCUSSION

7.1. *Comparison with the Observed X-Ray Properties*

In Figure 14, just analogous to Figure 1, we plot the X-ray luminosity at $t = 15$ Gyr of all the models presented in §§ 4 and 5, plus that of a number of other models specifically constructed for this display, and characterized by $0.75 \leq \chi \leq 1.1$ and various optical luminosities. All these additional models are either in their wind or in their outflow phase. A comparison between these two figures reveals the degree of success of the present class of evolutionary sequences in accounting for the observed average trend of L_X with L_B, as well as for large dispersion of L_X for intermediate values of L_B. It is worth recalling that such agreement with the observations is primarily the result of having constrained the model parameters to give χ values about unity, i.e., of having adopted the dark matter halo to be some 10 times more massive than the visible matter when the standard SN rate is assumed. We note that adopting a lower discrete source contribution $L_{\rm dscr}$ would appreciably affect only the wind models in Figure 14, lowering their L_X by virtually the same amount. Therefore, the good agreement between the present models and the observations would be preserved even adopting the low $L_{\rm dscr}$ contribution advocated by Forman et al. (1985). Figure 14 also indicates a remarkable prevalence of outflows, with the X-ray faint galaxies (those with $L_X \simeq L_{\rm dscr}$ in Fig. 1) being still in their wind phase and perhaps only a handful among the brightest galaxies having already experienced the transition to the inflow phase. We conclude that this class of models is able to naturally

© American Astronomical Society • Provided by the NASA Astrophysics Data System

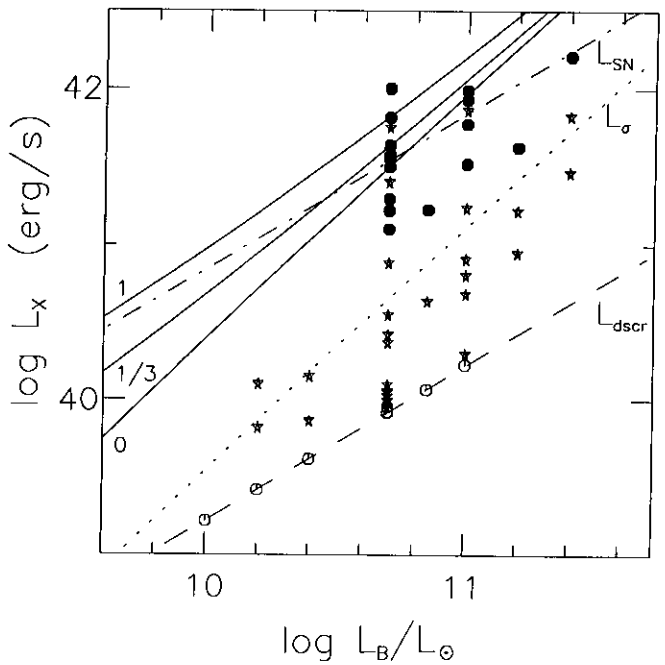

FIG. 14.—The X-ray vs. blue luminosity for a set of model galaxies at $t = 15$ Gyr, in the same format as Fig. 1; L_X includes the expected contribution from discrete sources (L_{dscr}). All the models in Tables 5 and 7 are reported, plus others constructed for this figure. Filled circles represent model galaxies which at $t = 15$ Gyr are in their inflow phase, stars and open circles represent outflowing and wind galaxies, respectively. Outflow galaxies which are brighter in X-rays than other inflow galaxies at the same L_B are such because caught in the verge of experiencing their central cooling catastrophe. On average the models follow the Faber-Jackson relation but some can deviate appreciably from the average relation, which explains why some models are brighter than L_{inflow}.

reproduce the richness of X-ray properties exhibited by real galaxies.

Besides integrated X-ray luminosities, there exists detailed X-ray surface brightness information for only three ellipticals, namely, NGC 4472, 4636, and 4649 (TFC; see also Sarazin & White 1988), which all show a $\Sigma_X(r)$ close to the optical profile. Again, cooling flow models give X-ray profiles which are systematically too centrally peaked compared to the observations, unless an ad hoc radial trend in star formation is postulated (Sarazin & Ashe 1989). On the contrary, our models exhibit a large variety of X-ray surface brightness profiles (see Fig. 6); in particular, models in the outflow phase are characterized by X-ray profiles which are very close or even wider than the optical profiles. Moreover, some outflow models exhibit $\Sigma_X(r)$ profiles which present a characteristic inflection also exhibited by the three TFC galaxies. The attempt of fitting with our models these specific objects is beyond the scope of the present paper, but in a future paper we will present evolutionary sequences in which the models are tailored to precisely reproduce the optical properties of the three galaxies. Given the extremely different profiles exhibited by models in the various evolutionary phases (winds, outflows with and without mini-inflows, and inflows), we anticipate the possibility of using the observed $\Sigma_X(r)$ profiles to identify the evolutionary state of individual galaxies, once that future X-ray observatories will have provided further data. In this perspective, in Paper I we have introduced the effective X-ray surface brightness $\Sigma_e = L_X/8\pi^2 R_X^2$, where R_X is the X-ray effective radius (inside which a luminosity $\frac{1}{2}L_X$ is sampled), as well as the effective X-ray surface brightness relative to the optical, $\Sigma'_e = L_X/(R_X/r_e)^2$. It will then become possible to organize synthetically the information concerning large numbers of ellipticals by making use of the $L_X - \Sigma'_e$ plane, which is somehow analogous to the classical H-R diagram, so helpful in stellar evolution studies. Evolutionary sequences in this plane, for various passbands of the X-ray detectors, will be presented in a future paper of this series.

In dealing with a multiparameter problem, the risk of having reproduced the observations by just fine-tuning a sufficient number of parameters must be carefully pondered. We believe that, by and large, this is not the case for the present study. Indeed, there are basically two main parameters controlling this class of solutions: the present value of χ and the parameter s describing the former evolution of the SN I rate. As we have seen, χ is constrained to be near unity in $L_B \simeq 5 \times 10^{10}\ L_\odot$ galaxies, if we want lower luminosity galaxies to be virtually devoid of gas as demanded by their low X-ray luminosity. Once low-luminosity galaxies are recognized as being in a wind phase, and high-luminosity galaxies are allowed to host an inflow, it becomes unavoidable to conclude that the bulk of galaxies—those at intermediate luminosities—ought to be in their outflow phase of evolution. We stress again that the condition $\bar{L}_{grav} \sim L_{SN}$ (i.e., $\chi \simeq 1$) follows directly from the observed properties of ellipticals, and it is indeed remarkable that disparate astrophysical processes, such as stellar mass loss, SN heating, and galaxy formation (the latter determining the depth of the potential well), all conjure to make L_{SN} of the same order of $\bar{L}_{grav}$.

Dark matter being not directly accessible to observations, the supernova parameters ϑ_{SN} and s become the two key factors of the problem, and once determined they can in turn set constraints on the dark matter. Crucial to our models are values of ϑ_{SN} within a factor of 2 or 3 from unity, and of s just in excess of ~ 1.3. What other astronomical evidences can be brought in support of such values? Concerning ϑ_{SN}, the current estimates of the SN I rate in ellipticals are just of this order, see § 2.3. Moreover, as discussed in the same section the present iron abundance in the flows provides a fairly direct measure of the SN I heating, via equation (10); see also Table 2. So, the strength of X-ray iron lines of elliptical galaxies can be used to provide a measure of the actual SN heating, as what matters in determining L_{SN} is the product $\vartheta_{SN} M_{Fe}$, which appears also in equation (10). Preliminary results from the *Ginga* satellite indicate an upper limit about twice solar for the iron abundance in the flows of NGC 4472 and NGC 4636 (Ohashi et al. 1990). This would imply $\vartheta_{SN} \lesssim 0.5$. Clearly, the actual detection of the iron lines, coupled to a detailed modeling of their emission, appears to be able to provide strong constraints on ϑ_{SN}, which can complement the traditional SN statistics.

For given value of ϑ_{SN}, the parameter s controls the evolution of the SN I rate over time and therefore the total number of SN I events occurred in a galaxy. In principle, the time evolution of the SN rate is accessible to observations by looking at progressively high-redshift galaxies, and pioneering studies in this direction are already under way (e.g., Nørgaard-Nielsen et al. 1989). Moreover, additional constraints (in particular on the parameter s) can be set by considering the total amount of iron contained in the hot intracluster medium of clusters of galaxies, and locked inside stars, which jointly represent a record of the past SN activity in galaxies. Indeed, the time integral of equation (7) gives the

© American Astronomical Society • Provided by the NASA Astrophysics Data System

number N of Type I SNs exploded up to the present, and therefore the total mass $M_{\rm Fe}^{\rm I}$ of iron produced by SN I's in the course of the whole evolution of the cluster galaxies. In this way, assuming that the cluster light is dominated by ellipticals, we get

$$M_{\rm Fe}^{\rm I} = NM_{\rm Fe} = 3.3 \times 10^{-3}\left(\frac{st_{015}^{1-s}-1}{s-1}\right)\vartheta_{\rm SN} M_{\rm Fe} L_B^{\rm cl} M_\odot , \quad (23)$$

where $M_{\rm Fe}$ ($= 0.6\ M_\odot$) is the mass of iron released by one SN I, $L_B^{\rm cl}$ is the total present luminosity of the cluster, and t_{015} is the initial time, before which equation (7) is not applicable, and we assume a constant SN I rate. We assume, t_{015} has to be of the order of the duration of the formation process of galaxies. For $s = 1.4$, the term in the parentheses on the right-hand side of equation (23) ranges from ~ 19 down to ~ 8 for t_0 in the range from 0.15 to 1 Gyr (i.e., the result is not much sensitive to the actual value of t_0), and we can take it to be ~ 10. Using equation (23), we thus introduce the predicted contribution of SN Is to the cluster *iron* mass to light ratio, which for $s = 1.4$ becomes $M_{\rm Fe}^{\rm I}/L_B^{\rm cl} \simeq 2 \times 10^{-2}\vartheta_{\rm SN}$ ($M_\odot/L_\odot$). Note that for $s = 0$, i.e., for a constant SN I rate, the cluster iron mass to light ratio is about an order of magnitude smaller.

Besides the contribution of Type I SNs, we need to estimate also the contribution of SNs produced by massive stars, which for convenience we call Type II. We assume that all stars initially more massive than 8 $M_\odot$ produce a SN II event and deliver 0.07 $M_\odot$ of iron. This value comes from the very precise determination obtained from the light curve of SN 1987A (Woosley 1988; Shigeyama, Nomoto, & Hashimoto 1988), and therefore it remains uncertain as to what extent the iron production in this event is representative of the weighted average over all SN II events. The total number of SN II events is obtained by integrating the IMF with the normalization obtained in § 2.1, and we obtain $(M_{\rm Fe}^{\rm II}/L_B) = 0.009$ and 0.004, respectively, for the single slope IMF with $x = 1.35$, and the multislope IMF with $x = 1.7$ for $M > 2\ M_\odot$, which provides a good representation of the Galactic IMF (Scalo 1986).

The iron produced by SNs of both types will now partly be locked into stars and partly will reside in the intracluster medium. In the present scenario, the SN II iron is produced during the early, actively star-forming phase in the evolution of the galaxies, and therefore most of it is likely to remain locked into stars. Conversely, the bulk of the stellar mass loss is ejected by galaxies during their wind phase, and this is even more so for the bulk of SN I produced iron (see Fig. 6 and Table 2). Thus the amount of iron subtracted by inflows is negligible, and most of the SN I iron flows directly into the intracluster medium. Stars in elliptical galaxies are generally regarded to be, on average, more metal rich than the Sun, and we conservatively assume the stellar iron mass fraction to be 0.002. Correspondingly, the stellar iron mass to light ratio becomes $(M_{\rm Fe}/L_B)_* = 0.002\ M_*/L_B$, or ~ 0.01, having adopted a stellar mass to light ratio of 5 (see Table 5). Therefore the iron produced by Type II SNs is barely sufficient to account for the iron which is now locked into stars, leaving room for a substantial contribution also from Type I SNs. Concerning the iron in the intracluster medium, in Table 8 we report the total blue luminosity, the iron abundance relative to solar abundance, the total amount of iron, and the iron mass to light ratios of three well-studied clusters. The iron abundance and $M_{\rm Fe}^{\rm cl}$ are from Rothenflug & Arnaud[3] (1985), while the references for the optical luminosities (corrected to $H_0 = 50$) are given in the note to Table 8. We note that the stellar and the cluster iron mass to light ratios are both $\sim 0.01\ M_\odot/L_\odot$, and the total is therefore ~ 0.02. SNs of Type II fall short of producing all the observed iron, unless the IMF slope is substantially flatter than Scalo's IMF (see also Mathews 1989). On the other hand, there is good agreement between predicted and observed iron mass to light ratios when SNs of Type I produce a major fraction of the total iron, which is indeed the case for the choice $s \simeq 1.4$–1.5 and $\vartheta_{\rm SN} \simeq 0.5$–1; i.e., for the values of the SN parameters we have adopted to model the gas flows in the galaxies. For $s = 0$, equation (23) implies a SN I contribution to the iron mass to light ratio of only ~ 0.002. If so, SN I's would be marginal contributors to the iron content of galaxies, compared to SN II's. This is at variance with the current understanding of the chemical evolution of galaxies, and in particular with the interpretation of the observed trend of the O/Fe ratio among halo stars (e.g., Matteucci & Greggio 1986; Abia, Canal, & Isern 1991). We conclude that our evolutionary models with declining SN I rate are in excellent agreement with observational constraints. Moreover, in models with early massive inflows most of the iron would be lost in the central sink of galaxies, rather than being delivered to the intracluster medium, where it is now observed.

TABLE 8

IRON MASS TO LIGHT RATIO OF CLUSTERS

Cluster	L_B ($10^{12}\ L_\odot$)	$Z^{\rm Fe}/Z_\odot^{\rm Fe}$	$M_{\rm Fe}^{\rm cl}$ ($10^{10}\ M_\odot$)	$M_{\rm Fe}^{\rm cl}/L_B$ ($M_\odot/L_\odot$)
Coma[a]	35	0.55	31	0.9×10^{-2}
Perseus[b]	12	0.50	19	1.6×10^{-2}
Virgo[c]	2.2	0.61	1.6	0.7×10^{-2}

[a] L_B from Dressler 1978.
[b] L_B from Bahcall 1974.
[c] L_B from van den Bergh 1977.

As noted in § 2.3, the iron abundance in the galactic winds can be several times solar, which is about one order of magnitude more than observed in the intracluster medium. This requires that early galactic winds had to be diluted with some 10 times larger mass of uncontaminated matter (with primordial abundances), thus implying a rather inefficient galaxy formation process, able to turn only a fraction ($\sim 10\%$–20%) of the baryonic matter into galaxies and stars. This result is consistent with that of Matteucci & Vettolani (1988), who have used the SN I rate constructed by Greggio & Renzini (1983). Compared to the value in Table 8, a much smaller value for the iron mass in the Perseus cluster has been recently advocated by Ponman et al. (1990), following the detection of an apparent gradient in the strength of the X-ray iron lines. If confirmed, this result could significantly affect the picture sketched above. A major loss of iron from the cluster (perhaps prior to its formation) would be required to reconcile this result with our preferred combination of the SN parameters $\vartheta_{\rm SN}$ and s.

7.2. *Fate of the Inflowing Gas during the Inflow Phase*

What happens to the inflowing gas during the inflow phase of these galaxies remains unanswered by the present set of

[3] We caution that these authors may have used a lower iron solar abundance than adopted in § 2.3. This does not affect our discussion here, since we are dealing with the total mass of iron, rather than its abundance in the intracluster medium.

© American Astronomical Society • Provided by the NASA Astrophysics Data System

evolutionary models, as it was in the case of steady state cooling flow models. However, in this respect there are two important differences between previous inflow models (including LM evolutionary models) and ours. First, according to the present picture only a few among the brightest ellipticals might have already experienced the transition to the inflow phase, and therefore only for a minority of galaxies the problem of the fate of the gas may actually exist. Second, even for those galaxies which are now hosting a gas inflow the problem is less severe than in models in which inflow dominates from the very beginning. Indeed, in our sequences the transition to the inflow is a rather late event in the evolutionary history of these galaxies, and it takes place when the bulk of stellar mass loss has already been ejected from the galaxy, mainly by the early supersonic wind. In this way the amount of material which disappears in the central sink is less than $\sim 10\%$ of the total stellar mass loss, i.e., of the amount which would have flown to the center in the case of persistent inflows. Therefore, less than $\sim 10^{10}\ M_\odot$ disappear (see Tables 5 and 7), as opposed to $\sim 10^{11}\ M_\odot$ as in the case of pure inflow models (see LM), and the inconsistency which caused major concern with LM models is considerably alleviated. Indeed, while it would be difficult to hide $\sim 10^{11}\ M_\odot$ of *dark* material within a galaxy's core radius, it would certainly be easier to do so with an amount 20 or 30 times smaller (Mathews 1988b).

Still the problem exists, although at a reduced scale. There is a vast literature on this issue, which to some extent is shared with the analogous question of cluster cooling flows onto central dominating (cD) galaxies (see Meiksin 1988, 1990; Sarazin 1986, and references therein). Local thermal instabilities causing a fraction of the gas to drop out of the flow locally have often been invoked as a remedy for both cluster and galaxy inflows (e.g., Fabian et al. 1986; Sarazin 1986), together with the additional conjecture that such instabilities would lead—preferentially if not exclusively—to the formation of low-mass, safely unobservable objects such as lower main-sequence stars, brown dwarfs, or jupiters. While we cannot disprove this ad hoc, virtually unfalsifiable solution, we find reasonable the exploration of other alternatives. In particular, for the case of individual elliptical galaxies, it remains merely conjectural that local thermal instabilities distributed throughout the whole galaxy can grow fast enough to avoid being devoured by the central maelstrom. This might be the case, but it has not been proved yet. In the frame of cooling-flow models much of the need for the ad hoc thermal instabilities and special IMF comes from the necessity of accounting for the low X-ray luminosity of most ellipticals (see § 2.5), coupled with the absence in them of clear signs of star formation. However, in the frame of our evolutionary models all this is automatically accounted for by the fact that in most galaxies there is no inflow at all, and therefore there is no excess energy to get rid of, and no star formation to hide. Therefore, there is no need to postulate local thermal instabilities and a special IMF.

However, if there is a moment during the evolution of our model galaxies when a burst of star formation seems more likely to occur, this is quite naturally the moment of the central cooling catastrophe, when a large amount of gas suddenly falls into the nucleus. At this time matter is cooling off at a rate up to $10\ M_\odot\ \mathrm{yr}^{-1}$, and quite rapidly $\sim 10^9\ M_\odot$ of cooled gas are accumulated. In our spherically symmetric simulation this gas disappears through the central sink, but in a more realistic situation it would probably settle in a dense disk (Cowie, Fabian, & Nulsen 1980), a few hundred parsecs in diameter, which may soon become gravitationally unstable and fragment into starlike objects. What if this happens with a standard IMF and a standard proportion of binaries? If the burst population is identical to the initial population of the galaxy, when it becomes 15 Gyr old it will reach the same stellar mass to light ratio of present galaxies, and therefore for total burst population mass of $10^9\ M_\odot$ the blue luminosity will be $5 \times 10^8\ L_\odot$, if we adopt $M_*/L_B = 5$. Note that this is the blue luminosity of the burst population when it has reached an age of 15 Gyr, while the burst itself will of course be much brighter. Inserting $L_B = 10^8\ L_\odot$ into equation (7), and from the relation $A = 2.9 L_B$, we get the proper normalizations for the Type I SN rate and for the IMF of the burst population. For the former quantity one has also to replace t_{15} with $t_{15} - t_{15}^{\mathrm{burst}}$, t_{15}^{burst} being the time at which the burst takes place. In such a way, we can estimate that a burst in which $\sim 10^9\ M_\odot$ of gas are turned into a population of stars with standard IMF ($x = 1.35$), and with a standard content of SN I progenitors will be able to produce some 5×10^7 stars more massive than $8\ M_\odot$ soon exploding as supernovae of Type II, and a Type I SN rate which will rival that of the whole galaxy for $\sim 10^9$ yr.

So, the central cooling catastrophe may coincide with a major optical display in the life of elliptical galaxies. Following Terlevich & Melnick (1988) and Terlevich (1990), a bursting object of this kind may exhibit several AGN–like properties, and it is tempting to speculate that the transition from the outflow to the inflow regime might be characterized by a brief AGN–like phase. What will happen later remains rather obscure. The fresh energy input from the Type II SNs of the burst population would be sufficient to unbound the X-ray gas of the galaxy (χ will drop below unity), and revert the inflow to a wind which will later slow down to an outflow, and the possibility of recurrent behaviors can be envisaged (see, e.g., Silk et al. 1986, for a similar suggestion). On the other hand, the additional Type I SNs from the burst population, with their slowly declining rate, could considerably delay a second cooling catastrophe, and few galaxies may experience more than one of such events in a Hubble time. There is, however, a difficulty with this otherwise attractive scenario. Reverting a cooling flow by heating it near the center can be a very inefficient process, as most of the heating may immediately go into radiation losses favored by the high gas density. Whether or not a wind is resuscitated will depend on the specific conditions which are established near the center, such as the detailed geometry of the disk and of the inflow, the actual SN rate, etc., i.e., on details which are inherently beyond the reach of our spherically symmetric models. There is, however, a last conjecture that we wish to advance. If the SN II activity associated with the burst and the longer lasting SN I tail are able to resuscitate an outflow and maintain it for several Gyr, then for several Gyr the resulting integrated spectrum of the galaxy will show the signs of a composite stellar population, with an intermediate-age, A-type–dominated population overlapping the old population of the galaxy. Such spectral characteristics have indeed been detected in several galaxies in medium-redshift clusters (the so-called E + A galaxies in Butcher-Oemler clusters; see Gunn & Dressler 1988; Dressler & Gunn 1990, and references therein), and these objects are indeed currently interpreted as postburst ellipticals. E + A galaxies may then represent a population of objects in their postcooling catastrophe evolutionary phase, and their X-ray properties may then systematically differ from those of normal ellipticals of the same luminosity. Star formation in zero–redshift ellip-

© American Astronomical Society • Provided by the NASA Astrophysics Data System

ticals have been occasionally invoked to account for the ultraviolet emission of these galaxies, a problem discussed in detail by Greggio & Renzini (1990) also in connection with the X-ray emission. They conclude that this possibility is not ruled out by presently available observations, but they also list and analyze a number of other alternatives offered by hot evolutionary stages of old, metal-rich stars.

A vast literature is concerned with gas inflow and accretion onto central black holes. We avoid here to address this problem in any detail, but it is worth emphasizing the large variety of accretion rates exhibited by our models, from only $\sim 10^{-2}\ M_\odot\ \mathrm{yr}^{-1}$ in dVG models with mini-inflows, up to $\sim 10\ M_\odot\ \mathrm{yr}^{-1}$ in galaxies which have just experienced the global cooling catastrophe. This may help interpreting the wide range in the strength of nuclear activity exhibited by elliptical galaxies and bulges. Finally, we note that estimating mass deposition rates by means of cooling flow models (e.g., Thomas et al. 1988) would give fallacious results if applied to outflowing galaxies, i.e., a large deposition rate would be indicated even when there is no mass deposition at all.

8. SUMMARY

In this paper we have considered the hydrodynamical evolution of spherically symmetric gas flows in elliptical galaxies, where the evolving ingredients are represented by the source terms, stellar mass loss, and supernova heating. Both King and de Vaucouleurs model galaxies have been studied, allowing for variable amounts of dark matter halos. In particular, we have investigated a class of evolutionary sequences characterized by a secularly declining rate of Type I SNs. The primary results found are as follows.

1. The gas flows in the model galaxies experience up to three consecutive evolutionary phases: the wind, outflow, and inflow phases. The first phase is characterized by supersonic winds, which decelerate until a subsonic outflow is established. The outflow phase can be maintained for many Gyr until a central cooling catastrophe triggers the transition to the inflow phase characterized by large infall velocities near the center, while in the outer parts the flows are close to hydrostatic equilibrium.

2. The amount of hot gas within the galaxies is subject to considerable changes during the various phases, decreasing during the wind phase, increasing during the outflow phase, and in general decreasing again during the inflow phase. A similar behavior is correspondingly followed by the X-ray luminosity of the model galaxies.

3. The epoch of the cooling catastrophe is extremely sensitive to the structural parameters describing the models, as well as to the adopted SN rate, and so is the present X-ray luminosity which reflects the amount of hot gas in the galaxies.

4. Good agreement with the observed trend of the X-ray luminosity L_X with the optical luminosity L_B and the velocity dispersion σ_* is achieved if in the bulk of the observed galaxies the supernova heating is close to the minimum required to steadily extract the gas from the galactic potential well. This provides an estimate for the amount of dark matter as a function of the adopted SN rate, which is of the order of 10 times the visible matter when the canonical SN rate is assumed.

5. The faintest X-ray galaxies are predicted to be still in their wind phase, while there is a prevalence of galaxies still in their outflow phase, and a few among the X-ray brightest galaxies may have already experienced the transition to the inflow phase. The use of cooling-flow models to diagnose flow properties of outflowing galaxies would indicate large inflow rates even where there is no inflow at all.

6. The large dispersion in L_X at given values of L_B is naturally accounted for in terms of modest galaxy-to-galaxy differences in any of the structural parameters, including small differences in the amount of dark matter and in its distribution.

7. The surface brightness distribution of the models is subject to major changes in the course of the evolution. During the wind phase it is narrower than the optical distribution, it becomes close or even wider than the optical during the outflow phase, and it dramatically shrinks during the inflow phase. The three galaxies for which detailed data are available appear to be in their outflow phase.

8. Models following de Vaucouleurs's stellar distribution differ in subtle details from those following King's density law. They are characterized by persistent mini-inflows which set in much before the global transition to the inflow regime. Such mini-inflows are confined to the inner few hundred parsecs and can be present even during the early supersonic wind phase. Mini-inflows should manifest as virtually pointlike X-ray sources located at the center of galaxies. Mini-inflows may also allow for some kind of nuclear activity even in relatively faint galaxies, provided that their central density is sufficiently high. It appears that partial wind (or partial outflow) configurations are more common among de Vaucouleurs's galaxies.

9. Hydrodynamical experiments show that a nonzero outer pressure (due to the intracluster gas) can have dramatic effects on the evolution of the flows of our spherically symmetric models. Important ram pressure effects are therefore anticipated in the case of real galaxies, particularly for those in the outflow evolutionary phase. Thermal conduction should be very effectively suppressed if the existence of powerful X-ray ellipticals is to be preserved in rich clusters.

10. As subsonic outflows are inherently unstable, on time scales of gigayears they may evolve to either winds or inflows under the action of tidal interactions or late merging events. It is speculated that a merging event may trigger an early transition to the inflow phase with the associated X-ray brightening. The claimed correlation between the boxiness parameter and L_X—if it exists—might be originated in this way. Alternatively, the correlation may originate from the binding energy per unit luminosity (actually L_{grav}/L_B) being systematically smaller in disklike galaxies.

11. It is argued that the iron abundance in the flows (as determined from X-ray iron lines) can be used to estimate the actual SN heating in ellipticals, thus offering an alternative way for the estimate of one of the main parameters controlling the evolution of the flows.

12. The total mass of iron in the intracluster medium represents a record of the integrated past SN activity in the individual galaxies and witnesses that most of the past stellar mass loss has been ejected from galaxies, rather than disposed in central sinks. The observed iron mass to light ratio of the clusters is quantitatively in excellent agreement with the declining SN I rate that we have assumed.

13. The fate of the infalling material when inflows are established remains the main open problem in the physics and astrophysics of galactic flows. However, in our evolutionary sequences the problem is much less severe than in traditional cooling-flow models, in that only a minor fraction of galaxies is predicted to have experienced a transition to the inflow phase, and even in this case the late establishment of an inflow ensures that much less matter is accumulated in the central regions.

© American Astronomical Society • Provided by the NASA Astrophysics Data System

14. The $L_X - L_B$ and $L_X - \sigma_*$ correlations are seen as an ongoing manifestation of the fact that brighter galaxies are characterized by a larger binding energy per unit mass, i.e., as an implication of the Faber-Jackson $L_B - \sigma_*$ relation, not unlike the L_B-metallicity correlation which is established at the formation epoch of elliptical galaxies. In this scenario, Type II SNs are responsible for the early establishment of galactic winds, and Type I SNs for their maintenance long after any star formation has ceased.

In the future this investigation will develop in various directions. In particular, we will further explore the parameter space and provide detailed surface brightness distributions of our models (also for passbands other than that of *Einstein*; e.g., *ROSAT*), and we will approach special phenomena which require a two-dimensional hydrodynamical treatment. This will include the interaction of the cold red giant wind with the hot ISM (so as to model the dust and Hα emission in these galaxies), and the interaction of evolving galactic flows with the intracluster gas (so as to study the ram pressure effects). We will also investigate about the evolution with lookback time of the X-ray luminosity of ellipticals, and the conditions under which the present class of evolutionary models may account for the higher proportion of E + A galaxies in moderately high redshift clusters.

We would like to thank Sperello di Serego Alighieri, George Djorgovski, Pepi Fabbiano, Sandra Faber, Laura Greggio, Garth Illingworth, David Koo, Beppe Longo, Bill Mathews, Avery Meiksin, Yoel Rephaeli, Craig Sarazin, Gustav Tammann, Guillermo Tenorio, Ginevra Trinchieri, and Paolo Vettolani for very useful conversations and/or for having kindly provided their preprints. A. R. also acknowledges the European Southern Observatory for its kind hospitality in a period during which part of this work has been developed, and for partial support the Italian Ministry of Research (MURST) and the Italian Space Agency (ASI) through the grant PSN 87037. We would also like to thank the personnel of the "CINECA" Computing Center for their assistance in the use of the Cray Y-MP 8/432.

REFERENCES

Abia, C., Canal, R., & Isern, J. 1991, ApJ, 366, 198
Anders, E., & Grevesse, N. 1989, Geochim. Cosmochim. Acta, 53, 197
Arimoto, N. 1989, in Evolutionary Phenomena in Galaxies, ed. J. E. Beckman, & B. E. J. Pagel (Cambridge Univ. Press), p. 323
Arimoto, N., & Yoshii, Y. 1987, A&A, 173, 23
Arnett, W. D., Branch, D., & Wheeler, J. C. 1985, Nature, 314, 337
Bahcall, N. A. 1974, ApJ, 187, 439
Bedogni, R., & D'Ercole, A. 1986, A&A, 157, 101
Bender, R., Surma, P., Döbereiner, S., Möllenhoff, C., & Madjesky, R. 1989, A&A, 217, 35
Bertola, F., Galletta, G., & Zeilinger, W. W. 1985, ApJ, 292, L51
Binney, J., & Tremaine, S. D. 1987, Galactic Dynamics (Princeton University Press)
Bragaglia, A., Greggio, A., Renzini, A., & D'Odorico, S. 1990, ApJ, 365, L13
Bregman, J. N., Roberts, M. S., & Giovanelli, R. 1988, ApJ, 330, L93
Buzzoni, A. 1989, ApJS, 71, 817
Canizares, C. R. 1988, in Cooling Flows in Clusters and Galaxies, ed. A. C. Fabian (Dordrecht: Kluwer), p. 376
Canizares, C. R., Fabbiano, G., & Trinchieri, G. 1987, ApJ, 312, 503 (CFT)
Cappellaro, E., & Turatto, M. 1988, A&A, 190, 10
Ciotti, L., & Pellegrini, S. 1991, in preparation
Cowie, L. L., Fabian, A., & Nulsen, P. E. J. 1980, MNRAS, 191, 399
Cowie, L. L., & Songaila, A. 1977, Nature, 266, 501
D'Ercole, A., Ciotti, L., Pellegrini, S., & Renzini, A. 1990, in Windows on Galaxies, ed. G. Fabbiano, J. A. Gallagher, & A. Renzini (Dordrecht: Kluwer), p. 275
D'Ercole, A., Renzini, A., Ciotti, L., & Pellegrini, S., 1989, ApJ, 341, L9 (Paper I)
di Serego Alighieri, S., Trinchieri, G., & Brocato, E. 1990, in Windows on Galaxies, ed. G. Fabbiano, J. A. Gallagher, & A. Renzini (Dordrecht: Kluwer), p. 301
Djorgovski, S., & Davis, M. 1987, ApJ, 313, 59 (DD)
Djorgovski, S., & de Carvalho, R. 1989, preprint
———. 1990, in Windows on Galaxies, ed. G. Fabbiano, J. A. Gallagher, & A. Renzini (Dordrecht: Kluwer), p. 307
Djorgovski, S., de Carvalho, R., & Han, M. S. 1989, in The Extragalactic Distance Scale, ed. S. van den Bergh & C. J. Pritchet, ASP Conf. Ser., 4, 329
Donnelly, R. H., Faber, S. M., & O'Connell, R. M. 1990, ApJ, 354, 52
Dressler, A. 1978, ApJ, 226, 55
Dressler, A., & Gunn, J. E. 1990, preprint
Dressler, A., Lynden-Bell, D., Burstein, D., Davies, R. L., Faber, S. M., Terlevich, R. J., & Wegner, G. 1987, ApJ, 313, 42 (7SI)
Evans, R., van den Bergh, S., & McClure, R. D. 1989, ApJ, 345, 752
Fabbiano, G. 1989, ARAA, 27, 87
Faber, S. M., & Gallagher, J. S. 1976, ApJ, 204, 365
Faber, S. M., & Jackson, R. E. 1976, ApJ, 204, 668
Faber, S. M., Wegner, G., Burstein, D., Davies, R. L., Dressler, A., Lynden-Bell, D., & Terlevich, R. J. 1989, Ap. J. Suppl., 69, 763
Fabian, A. C., Nulsen, P. E. J., & Canizares, C. R. 1984, Nature, 311, 733
Fabian, A. C., Thomas, P. A., Fall, S. M., & White, R. E., III, 1986, MNRAS, 221, 1049
Forman, W., Jones, C., & Tucker, W. 1985, ApJ, 293, 102
Forman, W., Schwartz, J., Jones, C., Liller, W., & Fabian, A. 1979, ApJ, 234, L27
Franx, M., & Illingworth, G. 1990, ApJ, 359, L41
Gaetz, T. J., Salpeter, E. E., & Shaviv, G. 1987, ApJ, 316, 530
Greggio, L., & Renzini, A. 1983, A&A, 118, 217
———. 1990, ApJ, 364, 35
Gunn, J. E., & Dressler, A. 1988, in Toward Understanding Galaxies at Large Redshift, ed. R. G. Kron & A. Renzini (Dordrecht: Kluwer), p. 227
Hattori, M., Habe, A., & Ikeuchi, S. 1987, Progr. Theor. Phys., 78, 1099
Hensler, G., & Burkert, A. 1990, in Windows on Galaxies, ed. G. Fabbiano, J. A. Gallagher, & A. Renzini (Dordrecht: Kluwer), p. 321
Iben, I., Jr., & Renzini, A. 1983, ARAA, 21, 271
Iben, I., Jr., & Tutukov, A. V. 1984, ApJS, 54, 335
Jura, M. 1990, in Windows on Galaxies, ed. G. Fabbiano, J. A. Gallagher, & A. Renzini (Dordrecht: Kluwer), p. 283
Landau, L. D., & Lifshitz, E. M. 1951, The Classical Theory of Fields (Oxford: Pergamon)
Larson, R. B. 1974, MNRAS, 166, 585
Lauer, T. 1985, ApJ, 292, 104
Loewenstein, M. 1989, MNRAS, 238, 15
———. 1990, ApJ, 349, 471
Loewenstein, M., & Mathews, W. G. 1987a, in Nearly Normal Galaxies, ed. S. M. Faber (New York: Springer-Verlag), p. 96 (LM)
———. 1987b, ApJ, 319, 614 (LM)
MacDonald, J., & Bailey, M. E. 1981, MNRAS, 197, 995
Mathews, W. G. 1988a, in Cooling Flows in Clusters and Galaxies, ed. A. C. Fabian (Dordrecht: Kluwer), p. 279
———. 1988b, AJ, 95, 1047
———. 1989, AJ, 97, 42
———. 1990, in Windows on Galaxies, ed. G. Fabbiano, J. A. Gallagher, & A. Renzini (Dordrecht: Kluwer), p. 265
Mathews, W. G., & Baker, J. 1971, ApJ, 170, 241
Mathews, W. G., & Bregman, J. N. 1978, ApJ, 224, 308
Mathews, W. G., & Loewenstein, M. 1986, ApJ, 306, L7 (ML)
Matteucci, F., & Greggio, L. 1986, A&A, 154, 279
Matteucci, F., & Vettolani, G. 1988, A&A, 202, 21
Meiksin, A. 1988, ApJ, 334, 59
———. 1990, in Windows on Galaxies, ed. G. Fabbiano, J. A. Gallagher, & A. Renzini (Dordrecht: Kluwer), p. 297
Mellier, Y., & Mathez, G. 1987, A&A, 175, 1
Mould, J. R., & Aaronson, M. 1985, ApJ, 303, 10
Mould, J., & Reid, N. 1987, ApJ, 321, 156
Nørgaard-Nielsen, H. U., Hansen, L., Jørgensen, H. E., Salamanca, A. A., Ellis, R. S., & Couch, W. J. 1989, Nature, 339, 523
Nulsen, P. E. J., Stewart, G. C., & Fabian, A. C. 1984, MNRAS, 208, 185
Ohashi, T., et al. 1990, in Windows on Galaxies, ed. G. Fabbiano, J. A. Gallagher, & A. Renzini (Dordrecht: Kluwer), p. 243
Ostriker, J. P. 1980, Comments Ap., 8, 177
Paczyński, B. 1970, Acta Astr., 20, 195
Peletier, R. F. 1989, Ph.D. thesis, University of Groningen.
Ponman, T. J., et al. 1990, Nature, 347, 450
Poveda, A. 1958, Bol. Obs. Tonantzitla Tacubaya, 17, 3
Renzini, A. 1988, in Planetary Nebulae, ed. S. Torres-Peimbert (Dordrecht: Kluwer), p. 259
———. 1989, in Evolutionary Phenomena in Galaxies, ed. J. E. Beckman & B. E. J. Pagel (Cambridge Univ. Press), p. 422
———. 1990, in Windows on Galaxies, ed. G. Fabbiano, J. A. Gallagher, & A. Renzini (Dordrecht: Kluwer), p. 255

© American Astronomical Society • Provided by the NASA Astrophysics Data System

Renzini, A., & Buzzoni, A. 1986, in Spectral Evolution of Galaxies, ed. C. Chiosi & A. Renzini (Dordrecht: Reidel), p. 135
Renzini, A., & Fusi Pecci, F. 1988, ARAA, 26, 199
Rephaeli, Y. 1987, MNRAS, 225, 851
Rothenflug, R., & Arnaud, M. 1985, A&A, 144, 431
Sadler, E. M. 1988, in Cooling Flows in Clusters and Galaxies, ed. A. C. Fabian (Dordrecht: Kluwer), p. 376
Sarazin, C. L. 1986, Rev. Mod. Phys., 58, 1
———. 1987, in IAU Symp. 117, Dark Matter in the Universe, ed. J. Kormendy & G. Knapp (Dordrecht: Reidel), p. 183
Sarazin, C. L., & Ashe, G. A. 1989, ApJ, 345, 22
Sarazin, C. L., & White, R. E., III. 1987, ApJ, 320, 32
———. 1988, ApJ, 331, 102
———. 1990, in Windows on Galaxies, ed. G. Fabbiano, J. A. Gallagher, & A. Renzini (Dordrecht: Kluwer), p. 279
Scalo, J. M. 1986, Fund. Cosmic Phys., 11, 1
Shigeyama, Y., Nomoto, K., & Hashimoto, M. 1988, A&A, 196, 141
Silk, J. 1989, ApJ, 345, L1
Silk, J., Djorgovski, S., Wyse, R. F., & Bruzual, G. 1986, ApJ, 307, 415
Sparks, W. B., & Macchetto, F. D. 1990, preprint
Takeda, H., Nulsen, P. E. J., & Fabian, A. C. 1980, MNRAS, 208, 279
Tammann, G. 1982, in Supernovae: A Survey of Current Research, ed. M. Rees & R. Stoneham (Dordrecht: Reidel), p. 371
Terlevich, R. 1990, in Windows on Galaxies, ed. G. Fabbiano, J. S. Gallagher, & A. Renzini (Dordrecht: Kluwer), p. 87
Terlevich, R., & Melnick, J. 1988, Nature, 333, 239
Thomas, P. A. 1986, MNRAS, 220, 949
Thomas, P. A., Fabian, A. C., Arnaud, K. A., Forman, W., & Jones, C. 1986, MNRAS, 222, 655
Tinsley, B. M. 1980, Fund. Cosmic Phys., 5, 287
Trinchieri, G., Fabbiano, G., & Canizares, C. R. 1986, ApJ, 310, 637 (TFC)
van den Bergh, S. 1977, Vistas Astr., 21, 71
———. 1991, Phys. Repts., in press
van den Bergh, S., & Tammann, G. 1991, ARAA, in press
van Leer, B. 1977, J. Comp. Phys., 23, 276
Vedder, P. W., Trester, J. J., & Canizares, C. R. 1988, ApJ, 332, 725
Weidemann, V. 1984, A&A, 134, L1
Whelan, J., & Iben, I., Jr. 1973, ApJ, 186, 1007
White, R. E., III, & Chevalier, R. A. 1983, ApJ, 275, 69
Wood, P. R., & Faulkner, D. J. 1986, ApJ, 307, 659
Woosley, S. E. 1988, ApJ, 330, 218
Woosley, S. E., & Weaver, T. A. 1986, ARAA, 24, 205

Note added in proof.—In a paper appeared after the acceptance of this paper (R. E. White III, 1991, ApJ, 367, 69) it is argued that Type II supernovae would be the major contributors to the iron content of clusters. The argument rests on an alleged oxygen overabundance in the intracluster gas, with an O/Fe ratio 3–5 times solar. However, with White's preferred combination of IMF slope and upper mass limit for SN II producers, the average iron production per SN II event is only $\sim 0.01\ M_\odot$ (~ 7 times smaller than what we have assumed) and the total number of SN II events ~ 2 times smaller. Correspondingly, the implied iron mass to light ratio $M_{\rm Fe}^{\rm II}/L_B$ is ~ 14 times smaller than the already small value we have derived in § 7.1, i.e., $\sim 0.004/14 \simeq 0.0003$, or 60–100 times less than the total iron mass to light ratio of the clusters (i.e., 0.02–0.03), stars and gas included. We conclude that either the iron production by massive stars is much larger than adopted by White or Type I events are indeed the major contributors. In this latter case it would be difficult to understand a large O/Fe ratio in the intracluster gas, and future X-ray observations of the oxygen and iron lines would be of great interest.

© American Astronomical Society • Provided by the NASA Astrophysics Data System